Journal of the Taiwan Institute of Chemical Engineers

Dissection of entropy production for the free convection of NEPCMs-filled porous wavy enclosure subject to volumetric heat source/sink

--Manuscript Draft--

Manuscript Number:	
Article Type:	SI:Nano-Renewable
Section/Category:	Energy and Environmental Science and Technology
Keywords:	NEPCMs; Fusion temperature; FEM; Entropy generation; Porous medium; Volumetric heat source/sink
Corresponding Author:	A.S. Dogonchi Aliabad Katoul, IRAN (ISLAMIC REPUBLIC OF)
First Author:	A.S. Dogonchi
Order of Authors:	A.S. Dogonchi
	S.R. Mishra
	Nader Karimi
	Ali J Chamkha
Abstract:	This study is dedicated to the inspection of the free convection of nanofluid as well as entropy generation inside a porous cavity loaded with nano-encapsulated phase change materials (NEPCMs). The wavy bottom section of the enclosure may be subject to a constant heat flux due to the transmitted sunlight comes from a parabolic trough solar collector. The volumetric heat source/sink is comprised in the governing equation. The robust finite element method (FEM) is deployed to handle the transformed governing equations and the numerical simulation of the streamlines and isotherms associated with velocity distribution for diverse factors are displayed. Further, the significant behaviour of the contributing parameters on the Nusselt and Bejan numbers are presented.
Suggested Reviewers:	M. Nawaz, PhD Institute of Space Technology nawaz@mail.ist.edu.pk
	Kai-Long Hsiao, PhD Taiwan Shoufu University hsiao.kailong@msa.hinet.net
	Abdelraheem M. Aly, PhD King Khalid University ababdallah@kku.edu.sa
	W.A. Khan, PhD Beijing Institute of Technology waqarazeem@bit.edu.cn
	Khalil Ur Rehman, PhD University of Waterloo kurrehman@uwaterloo.ca
Opposed Reviewers:	

COVER LETTER FOR SUBMISSION OF MANUSCRIPT

Subject: **Submission of manuscripts**

Dear Editor,

With this letter, I have attached a copy of manuscript entitled "**Dissection of entropy production for the free convection of NEPCMs-filled porous wavy enclosure subject to volumetric heat source/sink**". It is declared that the work described has not been published previously, that it is not under consideration for publication elsewhere, that its publication is approved by all authors and that, if accepted, it will not be published elsewhere in the same form, in English or in any other language, without the written consent of the Publisher.

With best wishes and highest personal regards.

Sincerely yours,

A.S. Dogonchi

Please check the following points before submitting the pdf file for your manuscript. Manuscripts that do not conform may be returned for correction and resubmission. You should be able to answer "yes" to all of the following questions.

- Is the manuscript double-spaced with a font size of 12 pt (Times or Times New Roman preferred)?

  YES

- Have you given full addresses and affiliations for all co-authors?

  YES

- Is the corresponding author identified by an asterisk (*) and their contact details (phone number and e-mail address) given on the first page?

  YES

- Have you given a Graphical Abstract and Highlights of your manuscript?

  YES

- Does the manuscript include a one-paragraph abstract of no more than 200 words for Original Papers or 150 words for Short Communications?

  YES

- Do the length of manuscript and the number of display items obey the requirement?

  YES

- Have keywords (maximum 6) been provided immediately after the abstract?

  YES

- Are sections given Arabic numbers with subsections numbered using the decimal system? NOTE: Acknowledgements and References sections are **not** numbered.

  YES

- Do you embed all figures, tables, and schemes (including the captions) at appropriate places in the text?

  YES

- Are References in the correct format for this journal?

  YES

- Are all references mentioned in the Reference list cited in the text, and vice versa?

YES

- Has the manuscript been spell-checked and grammar-checked?

  YES

- Are all symbols translated correctly in the pdf file?

  YES

- Has written permission been obtained and uploaded as Additional Files for use of copyrighted materials from other sources (including illustrations, tables, text quotations, Web content, etc.)? Has the copyright information been included in the relevant figure caption or table footnote, as an example "Reprinted with permission from Ref. [10]. Copyright 2010 Elsevier"?

  YES

Research Highlights:

- Free convection of NEPCMs along with entropy generation in an enclosure is dissected.
- The porous wavy enclosure may well be subject to a volumetric heat source/sink.
- The structure of the wavy part varies based on its undulation number and amplitude.
- The finite element method may well be applied to solve the governing equations.

Dissection of entropy production for the free convection of NEPCMs-filled porous wavy enclosure subject to volumetric heat source/sink

A. Sattar Dogonchi[1*], S.R. Mishra[2], Nader Karimi[3], Ali J. Chamkha[4,5]

[1]Independent researcher in Mechanical Engineering
[2]Siksha 'O' Anusandhan University, Bhubaneswar, Odisha 751030, India,
[3]School of Engineering and Materials Science, Queen Mary University of London, London, United Kingdom,
[4]Faculty of Engineering, Kuwait College of Science and Technology, Doha District, Kuwait,
[5]Center of Excellence in Desalination Technology, King Abdulaziz University, P.O. Box 80200, Jeddah 21589, Saudi Arabia,
***Corresponding author(s):** A. Sattar Dogonchi
(Email address: a.s.dogonchi@gmail.com, phone number: +98112707743)

ABSTRACT:

This study is dedicated to the inspection of the free convection of nanofluid as well as entropy generation inside a porous cavity loaded with nano-encapsulated phase change materials (NEPCMs). The wavy bottom section of the enclosure may be subject to a constant heat flux due to the transmitted sunlight comes from a parabolic trough solar collector. The volumetric heat source/sink is comprised in the governing equation. The robust finite element method (FEM) is deployed to handle the transformed governing equations and the numerical simulation of the streamlines and isotherms associated with velocity distribution for diverse factors are displayed. Further, the significant behaviour of the contributing parameters on the Nusselt and Bejan numbers are presented.

Keywords: NEPCMs; Fusion temperature; FEM; Entropy generation; Porous medium; Volumetric heat source/sink

1. Introduction

An immense application of nanomaterials is rendered in various fields of science and engineering as well as in various industries. Due to varied use of nanofluid as a best coolant the young researchers have keen interest to carry out their investigation in this direction. The fact is that nanofluid have greater thermal conductivity in comparison to the conventional fluids which may result in higher heat transfer performance. Nanofluids might well have utilization in diverse applications the most paramount of which could be solar collectors, medical applications, electronic cooling, and radiators [1-4]. At the same time, the exploration of natural convection (NC) which is one the substantial types of convective heat transmission in various applications for instance heat exchangers and geothermal systems along with nanofluids engrossed all researchers' attention. The impact of the heat source's movement on the NC within a triangle-shaped enclosure loaded with CuO-H_2O nanoliquid and considering the Brownian motion has been explored by Ghasemi and Aminossadati [5]. In another work, they [6] have also carried out numerical simulations to inspect the influence of disparate parameters like inclination angle on the heat transfer features of NC inside an inclined cavity taken up with the same nanoliquid. Numerical analysis of NC within a porous container with wavy wall and considering Brownian motion was conducted by Sheremet et al. [7]. They proved that the considered heat source may play a prominent role in the outcomes. Izadi et al [8] inspected numerically the influence of diverse arrangement of heat source on the NC inside a C-shaped nanoliquid-filled enclosure. The analysis of NC within a nanoliquid-loaded enclosure embodies a cross figure was conducted by Ahmed and Aly [9]. This study ascertained that diminishing the length of the cross figure by 0.6 may result in an enhancement in the amount of stream function by almost 28%. Ma et al. [10] perused the problem of NC for a MWCNTs-H_2O nanoliquid inside a U-shaped cavity that possesses a hot hurdle. Their outcomes demonstrated that at lower Rayleigh number (Ra) placing the hot hurdle in the right or left sides of the enclosure could cause the highest Nusselt number (Nu). Magnetic NC and entropy generation (EG) of ferroliquids within a container embodies horizontal sheet was examined by Sivaraj and Sheremet [11]. The most important outcome of this work was lessening the Hartmann number (Ha) may result in an enhancement in the mean Nu and EG. Seyyedi [12] scrutinized the EG for a natural convection of nanoliquid within a heart-shaped porous container under magnetic field. Eccentricity influence of heat source inside a porous region on the NC and EG of nanoliquid was inspected by Gholamalipour et al. [13]. The impacts of diverse types of barriers, interior heat generation, and magnetic field on the NC and EG within a nanoliquid-filled enclosure have been explored by Selimefendigil and Oztop [14]. Their explorations determined that the existence of hurdles could worsen the heat transmission procedure. Rashad et al. [15] analyzed the influence of the position and size of the heat sink/source on the entropy generation and magnetic NC for a nanoliquid within an inclined porous container. Cho et al. [16] carefully examined the NC for the Al_2O_3-H_2O nanoliquid-filled enclosure with wavy-side-walls. They proved that ascending the volume fraction of nanomaterials may cause an increment in the Nu for each Ra. The EG and heat transmission features for a hybrid nanoliquid during NC process among two oval cylinders was inspected by Tayebi and Oztop [17]. They reported the majority of entropy production at lower Ra is owing to thermic irreversibility.

Nowadays researchers are focusing on the new type of nanoliquids called nano-encapsulated phase change materials (NEPCMs). In this kind of nanoliquids a core as well as a shell are constituents of the nanomaterials and The former which is prepared by using phase change material (PCM) may witness a solid-liquid phase alteration at a determined fusion temperature and consequently it might well either take in or discharge a considerable quantity of energy because of the latent heat of the phase alteration [18,19]. Ghalambaz et al. [19] perused the NC features for the NEPCMs-filled cavity and their outcomes proved that dimensionless fusion temperature could play a leading role in the growth of heat transfer. Raizah and Aly [20] conducted a research on the suspension of the NEPCMs for the double-diffusive convection flow within a porous enclosure. They deduced that the ascending the concentration of nanomaterials could improve the phase alteration region. Seyf et al. [21] examined the hydrodynamic and thermic features of microtube heat sink by taking NEPCMs slurry into account as coolant. Their study ascertained a growth in NEPCMs's melting range could lead to an enhancement in the Nu. Ghalambaz et al. [22] inspected the EG for a natural convection of NEPCMs inside a semi-annular container. They revealed the heat transfer may boost by existence of the particles of NEPCMs. The influence of Stefan number on the NC within a NEPCMs-filled eccentric region was scrutinized by Mehryan et al. [23]. The results demonstrated that in the case of lower Stefan number more heat transfer could be achievable. The analysis of the entropy production for a magnetic NC within a NEPCMs-loaded porous container entails rectangular fins was conducted by Dogonchi et al. [24]. They acquired the fins could have a remarkable impact of the features of heat transfer.

This work dissects the entropy generation along with natural convection within a NEPCMs-filled porous enclosure in which its wavy bottom part which may vary according to the undulation number and amplitude is subject to a constant heat flux because of the transmitted sunlight comes from a parabolic trough solar collector (PTSC). Considering the volumetric heat source/sink, the governing equations may well be solved via finite element method (FEM) and accordingly the results may be portrayed for disparate governing parameters.

2. Governing Equations

A parabolic trough solar collector (PTSC) with a reflector that could transmit the sunlight to the bottom part of the porous enclosure subject to volumetric heat source/sink and filled up with NEPCMs in which the natural convection takes place is analysed in the current investigation (Figure-1). The structure of the wavy part of enclosure subject to a constant heat flux could vary based on its undulation number and amplitude. The fluid flow may well be assumed to be steady, laminar, Newtonian, and incompressible. Therefore, taking account of Boussinesq theory the equations governing on this kind of system could be represented as:

$$\frac{\partial u}{\partial x}+\frac{\partial v}{\partial y}=0 \tag{1}$$

$$\rho_b\left(v\,\frac{\partial u}{\partial y}+u\,\frac{\partial u}{\partial x}\right)=\mu_b\left(\frac{\partial^2 u}{\partial x^2}+\frac{\partial^2 u}{\partial y^2}\right)-\frac{\partial p}{\partial x}-\frac{\mu_b}{K}u \tag{2}$$

$$\rho_b\left(v\,\frac{\partial v}{\partial y}+u\,\frac{\partial v}{\partial x}\right)=\mu_b\left(\frac{\partial^2 v}{\partial y^2}+\frac{\partial^2 v}{\partial x^2}\right)-\frac{\partial p}{\partial y}-\frac{\mu_b}{K}v+g\,\rho_b\beta_b\left(T-T_c\right) \tag{3}$$

$$\left(u\,\frac{\partial T}{\partial x}+v\,\frac{\partial T}{\partial y}\right)=\frac{k_b}{\left(\rho C_p\right)_b}\left(\frac{\partial^2 T}{\partial x^2}+\frac{\partial^2 T}{\partial y^2}\right)+\frac{Q_0}{\left(\rho C_p\right)_b}\left(T-T_c\right) \tag{4}$$

In order to gain the dimensionless form of these equations, some parameters must be determined which could be expressed as:

$$X=\frac{x}{L},\quad \theta=\frac{T-T_c}{T_h-T_c},\quad Y=\frac{y}{L},\quad V=\frac{vL}{\alpha_f},\quad U=\frac{uL}{\alpha_f},\quad P=\frac{pL^2}{\rho_f\,\alpha_f^2} \tag{5}$$

by doing so the governing equations in their dimensionless structure would be written as:

$$\left(U\,\frac{\partial U}{\partial X}+V\,\frac{\partial U}{\partial Y}\right)=-\frac{1}{\rho_b/\rho_f}\frac{\partial P}{\partial X}+\frac{\mu_b/\mu_f}{\rho_b/\rho_f}\Pr\left(\frac{\partial^2 U}{\partial X^2}+\frac{\partial^2 U}{\partial Y^2}\right)-\frac{\mu_b/\mu_f}{\rho_b/\rho_f}\frac{\Pr}{Da}U \tag{6}$$

$$\begin{aligned}\left(V\,\frac{\partial V}{\partial Y}+U\,\frac{\partial V}{\partial X}\right)=+\frac{\mu_b/\mu_f}{\rho_b/\rho_f}\Pr\left(\frac{\partial^2 V}{\partial X^2}+\frac{\partial^2 V}{\partial Y^2}\right)-\frac{1}{\rho_b/\rho_f}\frac{\partial P}{\partial Y}\\ -\frac{\mu_b/\mu_f}{\rho_b/\rho_f}\frac{\Pr}{Da}V+\frac{\beta_b}{\beta_f}\Pr Ra\theta\end{aligned} \tag{7}$$

$$C_r\left(U\,\frac{\partial \theta}{\partial X}+V\,\frac{\partial \theta}{\partial Y}\right)=\left(k_b/k_f\right)\left(\frac{\partial^2\theta}{\partial X^2}+\frac{\partial^2\theta}{\partial Y^2}\right)+Hs\cdot\theta \tag{8}$$

here $\rho_b/\rho_f=\left(1-\phi\right)+\phi\left(\rho_p/\rho_f\right)$, $\beta_b/\beta_f=\left(1-\phi\right)+\phi\left(\beta_p/\beta_f\right)$, $\mu_b/\mu_f=\left(1+N_v\phi\right)$, $k_b/k_f=\left(1+N_c\phi\right)$, and $C_r=\left(\rho C_p\right)_b/\left(\rho C_p\right)_f=\left(1-\phi\right)+\phi\lambda+\frac{\phi}{\chi Ste}f$. In the last three expressions N_v, N_c, *Ste*, and *f* implicate the numbers of dynamic viscosity and thermal conductivity, the Stefan number, and the dimensionless fusion function, respectively. According to [19], *f* may well be expressed as:

$$f = \frac{\pi}{2}\sin\left(\frac{\pi}{\chi}\left(\theta-\theta_f+\frac{\chi}{2}\right)\right)\times\begin{cases}0 & \theta<\theta_f-\frac{\chi}{2}\\ 1 & \theta_f-\frac{\chi}{2}<\theta<\theta_f+\frac{\chi}{2}\\ 0 & \theta>\theta_f+\frac{\chi}{2}\end{cases} \quad (9)$$

in which θ_f represents the dimensionless fusion temperature.

Furthermore, the following boundary conditions are considered for the current paper:

$$\begin{array}{llll}\Psi=0 & \text{on all walls,} & \theta=0 & \text{on the cold wall}\\ \partial\theta/\partial n=-1 & \text{on the heated wall} & \partial\theta/\partial n=0 & \text{on the adiabatic walls}\end{array} \quad (10)$$

The heat transfer rate i.e. the local and average Nusselt numbers on the heated wall could be ascertained as:

$$Nu_{loc.}=\frac{k_b}{k_f}\frac{\partial\theta}{\partial n},\ Nu_{ave.}=\frac{1}{S}\int_0^S Nu_{loc.}ds \quad (11)$$

in the above-mentioned equations S designates the length of wall which is subject to the constant heat flux.

3. Entropy generation

In this section the equations required to dissect the entropy generation (En) for the current system could be demonstrated as [25]:

$$En_{local} = \underbrace{(1+N_c\phi)\left[\left(\frac{\partial\theta}{\partial Y}\right)^2+\left(\frac{\partial\theta}{\partial X}\right)^2\right]}_{En_{local,HT}} + \underbrace{(1+N_v\phi)\varepsilon_f\left[\begin{array}{l}2\left(\frac{\partial U}{\partial Y}\right)^2+2\left(\frac{\partial U}{\partial X}\right)^2\\ +\left(\frac{\partial U}{\partial X}+\frac{\partial U}{\partial Y}\right)^2\end{array}\right]}_{En_{local,FF}} + \underbrace{(1+N_v\phi)\frac{\varepsilon_f}{Da}\left(U^2+V^2\right)}_{En_{local,PM}} \quad (12)$$

here $En_{local,\ HT}$, $En_{local,\ FF}$, and $En_{local,\ PM}$ signify the local entropy generation because of heat transfer, fluid friction, and porous medium, respectively and the aggregate of them would result in the local entropy generation En_{local}. Moreover, the total entropy generation may well be attained by integrating them as:

$$\begin{array}{ll} En_{total,HT} = \int_V En_{local,HT}\,\mathrm{dV}. & En_{total,FF} = \int_V En_{local,FF}\,\mathrm{dV}. \\ En_{total,PM} = \int_V En_{local,PM}\,\mathrm{dV}. & En_{total} = \int_V En_{local}\,\mathrm{dV}. \end{array} \quad (13)$$

4. Numerical approach and validation

The proposed article is formulated on the flow of nanoliquid inside a porous cavity filled loaded NEPCMs. The wavy bottom section of the enclosure may be subject to a constant heat flux due to the transmitted sunlight comes from a parabolic trough solar collector (**Fig.1**). The volumetric heat source/sink is included in the governing equation. The impact of permeability may also be inspected to deliberate the credibility of the resistive force on the flow phenomena of the nanofluid. The distorted coupled equations (6-8) associated with the fusion function and the appropriate boundary conditions (10) are solved numerically by employing finite element method. A non-uniform structural grid is prepared and then the governing equations presented in its weak forms discretized. Moreover, the iteration procedure may be carried on till to gain a good precision of 10^{-5}. More explanations about the procedure could be found from [26]. In order to figure out the accuracy of this method, we made a comparison between the outcome of it with those of Krane, and Jessee [27], the experimental work and the work of Khanafer et al.[28] for a quadrangular cavity filled up with nanoliquid and the consequence of this assessment displayed in **Fig.2** proved that the results of FEM could be trustable.

5. Results and discussion

The role of nanoparticle volume fraction, ϕ is vital for the enhancement of the heat transfer properties since the effective thermal properties such as viscosity, density, conductivity and the volumetric expansions are dependent upon the volume fraction of the nanoparticle. However, the dynamic viscosity N_v, thermal conductivity, N_c and the Stefan number, *Ste* are also have vital role on the heat transfer phenomenon. Further, the fusion function f with an involvement of dimensionless fusion temperature, (θ_f), has significant contributions on it. Besides to that the influence of diverse parameters for instance Rayleigh number (*Ra*), heat source parameter (*Hs*), Darcy number (*Da*), and the undulation number (*N*) of wavy wall and its amplitude (*b*) on the natural convection features happened inside a NEPCMs-filled porous cavity subject to constant heat flux is scrutinized via graphically and the numerical simulation of the average Nusselt number is presented in tabular form. **Table 1** portrays the impact of Da and Ra in conjunction with ϕ on the profiles of average Nusselt number, Nu_{ave}. The simulated is carried out for several values of Ra i.e. Ra=10^3, Ra=10^5 and Ra=10^5 by introducing various values of the Da. The range of the nanoparticle volume fraction is considered to be 1% to 5%. Volume fraction is the amount of nanoparticle present in the base fluid that is completely agglomerated. The augmentation in ϕ renders to a significant hike in Nu_{ave} and the greater in the strength of Da. This behaviour is exhibited because of the body force's resistance appeared by the flow of nanofluid within the permeable medium that enhances the heat transmission rate about the cold area. Further, enhanced Ra boosts up the profile as a result the Nu_{ave} grows. Moreover, the influence of various pertinent physical parameters with fixed values of the remaining deliberated earlier, the profiles of fluid temperature θ, streamlines Ψ, heat capacity ratio C_r and the velocity is presented graphically. **Fig.3** portrays the characteristics of *Da* and *Ra* on the C_r, θ, and Ψ contours. The range of Rayleigh number is assumed to be $10^3 < Ra < 10^5$. An increase in the *Ra* the fluid temperature boosts up which cause the contour to move to the top from the bottom layer to the central part of the channel. The adiabatic region leaves the temperature that causes a significant enhancement in the temperature. This happens owing to a growth in *Ra*. However, without the loss of generality an enhanced permeability enforces to give rise to the temperature contour. It is seen that for *Da* =10^{-1}, the alteration of $|\Psi_{\max}|_{nf}$ is displayed with its ascending treatment as 0.0430446 to 3.42847, for *Da* = 10^{-2}, it rises from $|\Psi_{\max}| = 0.0309333$ to $|\Psi_{\max}| = 3.00692$ and finally for *Da* =10^{-3} this variation is encountered as $|\Psi_{\max}| = 0.00832293$ to $|\Psi_{\max}| = 0.788381$. Further, growing Da may cause flow field to weak. This would be owing to the fact that the incorporation of resistive force leads a retarding effect. The impact of *Ra* and *Da* on the velocities distribution (U,V) due to the inclusion of 5% nanoparticle volume fraction is presented in **Fig.4**. Irrespective of the permeability of the medium increasing *Ra* could lead to *U* and *V* to enhance in their own orientations. However, increment in Da, the velocities distribution retards remarkably for the several amounts of Ra. The forces i.e. inclusion of porosity could oppose the velocity distribution. However, separation near the vertical walls of the cavity is exhibited due to the hot and cold walls. The variation of the heat source/sink due to the enhanced values of the Ra on the fluid temperature, streamlines and the heat capacity ratio contour profiles is displayed in **Fig.5**. The significant enhancement is encountered in the temperature distribution of the nanofluid for the suitable temperature differences from sink to source. The range of the level of changes in the absorption to heat generation is -3 to 3 i.e. $-3<Hs<3$. As described earlier the boosts in the profiles is rendered for greater values of *Ra*. However, the fixed values of the other pertinent parameters are exhibited in the corresponding profiles. **Fig.6** illustrates the variation of heat source/sink on the velocity profiles of both longitudinal and transverse direction. The significant improvement in the velocity distributions is marked for the level of changes in the external heat applied to the system. In the permeable medium the velocity profiles boosts up when the range of the heat source/sink varies from -3 to 3. It is seen that, the variation of longitudinal velocity is from $|U_{max}| = 0.205589$ to $|U_{max}| = 0.728494$ and transverse velocity from $|V_{max}| = 0.25332$ to $|V_{max}| = 0.347443$ for $Ra=10^3$. Similarly, drastically improvement is rendered for the higher values of *Ra* as displayed in the corresponding figure. **Fig.7** and **Fig.8** describe the variation of the undulation number (*N*) of wavy wall and its amplitude (*b*) on the various profiles of temperature, streamlines, C_r and the velocity distribution of both longitudinal and transverse profiles respectively. The variation of *b* is observed within the range of 0.1 to 0.3 whereas the undulation number (*N*) considered as *N=1*, *N=2* and *N=3*. It is interesting to observe that with increasing *N* the number of wave forms near the heat flux region varies depending upon *N* and there is a similar pattern follows in each profiles. Further, it is seen that enhancing amplitude encourages to grown up the profile significantly. This pattern changes highly with enhanced values of Ra from the bottom layer towards the upper region of the semi-circular cavity. Further, significant augmentation in the velocity profile is marked due to enhanced values of both b and N. The fusion temperature has significant role on the Cr is exhibited in **Fig.9** for several enhancement in the values of Ra. Here, the fusion function depends upon the fusion temperature that is varies within the range $0.1< \theta f <0.4$ and it is seen that increasing θf the lower down the profile from the upper part of the cavity to the bottom layer and it gradually diminishes at the bottom layer for the low values of Ra i.e. $Ra =10^3$. For the higher Ra it is observed that the, near the inner wall of the cavity it gives rise due to the energy dissipates from the core shell of the PCM and for constant heat flux applied thereat. The irreversibility of the system due to the simulation of thermal energy causes a significant study on the entropy generation. The measure of the thermal energy per unit temperature is called Entropy which also measures the molecular disorder. **Fig. 10** signifies the variation of $En_{local,\ HT}$, $En_{local,\ FF}$, and $En_{local,\ PM}$ i.e. the local entropy generation because of heat transfer, fluid friction, and porous medium for the several values of Da along with the higher values of *Ra*. It is seen that the core part of the cavity a significant change in the local entropy is rendered due to heat transfer and further it distributes throughout the cavity for increasing *Ra*. No significant deviation is marked in the local entropy due to the fluid friction however, it affects the profiles of local entropy due to the permeability of the medium. However, the pressure drop in the cavity signifies the Bejan number. The simulation of Be_{local} for diverse values of Ra in a specified range of Da is portrayed in **Fig.11**. One may deduce that the local Bejan number descends with growing Ra also ascending Da and porosity with higher Rayleigh number, the treatment of the local Bejan number is negligible. Significance of the Rayleigh number on the profiles of variation of $En_{local,\ HT}$, $En_{local,\ FF}$, and $En_{local,\ PM}$ i.e. the local entropy generation because of heat transfer, fluid friction, and porous medium for the several values of the different values of heat source/sink that is presented in **Fig.12**. It is noteworthy that, for the lower value of *Ra* the distribution is located near the inner walls and further increasing values of *Ra* enhance the transfer rate throughout the entire domain. However, the enhanced values of *Hs* from sink to source the local entropy for the heat transfer is located near to the inner walls. Further, increasing *Ra* the distribution of the entropy in the permeable medium is higher than that of the lower values of *Ra*. **Fig.13** deliberates the local entropy as well as the local Bejan value for the values of *Ra* and heat source/sink. Earlier it is described as the local entropy located near the inner wall for the lower values of *Ra* and further it distributes throughout the cavity it is pointed out the impact is reverse in case of local Bejan value. Henceforth, for the lower values of *Ra* the distribution is located near the outer walls and then gradually transfer towards the entire cavity as *Ra* increases. The behaviour of undulation number (*N*) of wavy wall and its amplitude (*b*) on the profiles of $En_{local, HT}$, $En_{local, FF}$, and $En_{local, PM}$ in **Fig.14** and the on the profiles of local entropy as well as the local Bejan in **Fig.15**. The heat transfer rate diminishes gradually as the enhancement of the N and b. For higher value of N, the entropy loss in case of HT and FF in ore whereas the effect is reverse in case of permeable medium. The observation for the case of local entropy and local Bejan number also decelerates for the increasing N and b. The heat transfer rate that is the $Nu_{loc.}$ versus length of the heater for various values of *Ra*, *Da* and *Hs* is presented in **Fig.16**. The behaviour of these parameters on the local rate coefficient is affected due to the augmentation in these values. It is seen that the in the permeable medium the change in Nusselt number is insignificant but in the impermeable region the deviation between the profile is significant for higher *Ra*. Also, it is interesting that near the outer walls a little bit hikes is marked and the similar retardation is presented in magnitude at the second wall. Moreover, in the middle region a simple fluctuation is occurred and almost at centre of the cavity a remarkable hike is pronounced. A similar characteristic is observed for the several values of the heat source/sink parameter. It is noticed that the increasing values of *Hs* from the sink to source retards the profile significantly. Again enhanced values of *Ra* the squeeze between the profiles augmented significantly. The profile of Nu_{loc} for the variation of the undulation number (*N*) of wavy wall, its amplitude (*b*), and *Ra* is observed in **Fig.17**. As described earlier, the pattern of the profiles is similar but the increasing *b* and *N* retards the local Nusselt number and the number of wavy front is displayed depending upon the values of *N*. **Fig. 18** illustrates the variation of *Da*, *Hs* and *Ra* on the Nu_{ave}. All the figures suggest the influence of *Da* and *Hs* versus *Ra* to measure the characteristics of Nu_{ave}. Initially for lower *Ra* i.e. as *Ra* varies from 10^3 to 10^4 the behaviour is approximately linear and further, drastic enhancement is rendered within the range 10^4 to 10^5. The retardation in the porosity i.e. $10^{-1}<Da<10^{-3}$ the rate of Nu_{ave} is greater. In comparison to *Hs* for both sink and source it is beneficial to the absorption coefficient that enhances the average Nusselt number. **Fig.19** illustrates the influence of the undulation number (*N*) of wavy wall and its amplitude (*b*) on the profiles of Nu_{ave} with respect to the proposed range of Rayleigh number. The profile increases slightly within the range of *Ra* from 10^3 to 10^4 but further for higher *Ra* i.e. from 10^4 to 10^5 the boost in the heat transfer rate in greater. However, the augmentation in the values of *b* retards the profiles significantly. The experience of the Stefan number and *Ra* versus fusion temperature on the Nu_{ave} is presented in **Fig.20**. It is seen that irrespective of the values of *Ra* the increasing Stefan number a hike is marked within the range of $\theta_f < 0.2$ and further it retards significantly. **Fig.21** and **Fig.22** displays the impact of *Da* and *Hs* respectively with respect to *Ra* on the various profiles of $En_{local, HT}$, $En_{local, FF}$, and $En_{local, PM}$ i.e. the local entropy generation because of heat transfer, fluid friction, and porous medium. The increasing values of *Ra* within the range 10^3 to 10^4 the profile retards insignificantly however, the sudden retardation is marked within the range 10^4 to 10^5 in case of total entropy due to heat transfer. The behaviour is reversed in case of the total entropy due to fluid friction and porous medium. Moreover, the appearance of heat source and sink also retards for lower values of *Ra* i.e. 10^3 to 10^4 for the total entropy due to heat transfer and impact is opposite in other three cases displayed in the Figure. **Fig.23** displays the behaviour of the undulation number (*N*) of wavy wall and its amplitude (*b*) on the profiles of $En_{local, HT}$, $En_{local, FF}$, and $En_{local, PM}$. Here, the variation of *b* versus *N* is displayed in each figure. It is noteworthy that the all the profiles of entropy enhance with increasing the amplitude with respect to the increasing undulation number for the existence of various Rayleigh number.

Closing remarks

The flow of nanofluid enclosed within a porous enclosure filled with NEPCMs is analysed in the current investigation. The wavy bottom section of the enclosure may be subject to a constant heat flux due to the transmitted sunlight comes from a parabolic trough solar collector. The volumetric heat source/sink is included in the governing equation. The absorption of NEPCM particle and release of latent heat are obtained due to the phase change material. Finite Element Method, a numerical scheme is utilized to solve governing equations and simulations may be conducted for controlling parameter. Further, the computational outcomes of entropy generation are portrayed by figures. All in all, the ultimate notable outcomes are;

- A greater concurrency of the present simulated result with that of the former experimental and numerical outcomes is obtained and that corroborates a path to lead this work for the further examination with an inclusion of contributing parameters employing the numerical evaluation scheme FEM.
- The heat transfer criterion enriches owing to the conjunction of thermal conductivity and heat capacity for fusion temperature with an inclusion of NEPCM.
- Higher Rayleigh number boosts up the profile of Nu_{ave} and further, growing in the nanoparticle volume fraction also encourages present. This behaviour is rendered due to the resistive force offered by the Darcy number.
- For the lower value of Ra the distribution is located near the inner walls and further increasing values of Rayleigh number enhance the transfer rate throughout the entire domain.
- The Nu_{avg} falls due to the flow through the permeable region and further augmenting Ra in its range, decelerates the profile of Nu_{avg} significantly.

Table 1. The alteration of $Nu_{ave.}$ with ϕ at diverse Ra and Da

Ra	Da	ϕ	$Nu_{ave.}$
10^3	10^{-1}	0.01	2.2102
		0.03	2.4879
		0.05	2.7828
	10^{-3}	0.01	2.2059
		0.03	2.4806
		0.05	2.7716
10^4	10^{-1}	0.01	2.3348
		0.03	2.6396
		0.05	2.9633
	10^{-3}	0.01	2.2190
		0.03	2.5019
		0.05	2.8031
10^5	10^{-1}	0.01	3.3732
		0.03	4.1968
		0.05	4.4436
	10^{-3}	0.01	2.6241
		0.03	2.9503
		0.05	3.2763

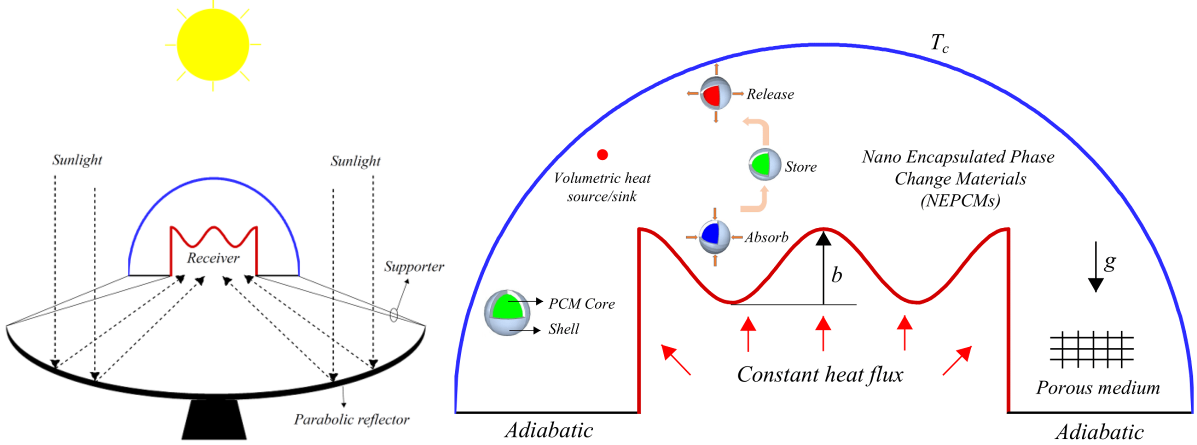

Fig. 1. Schematic of current work

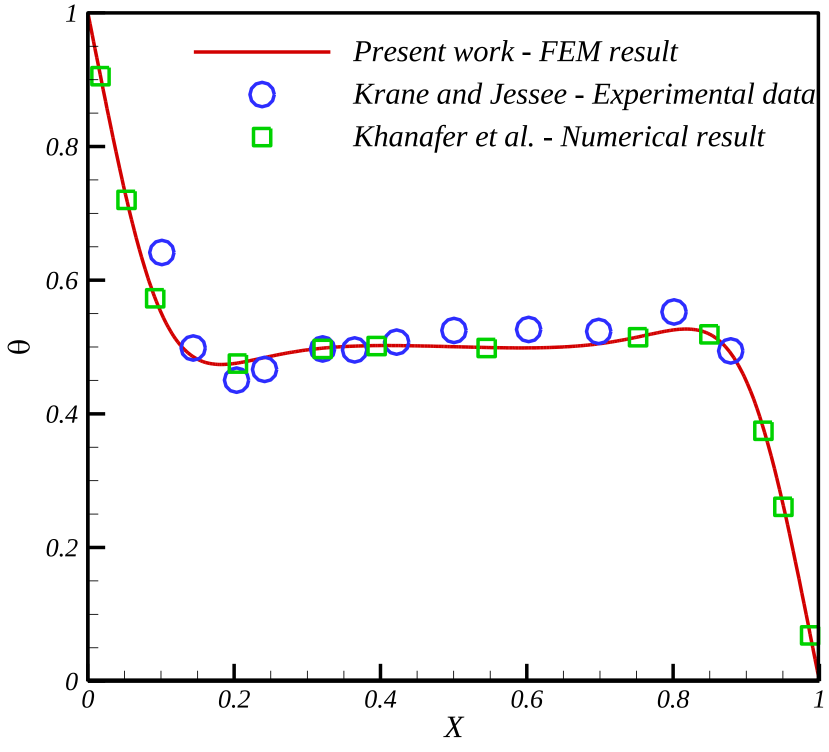

Fig. 2. Confirmation of present work with experimental [3] and numerical results [4]

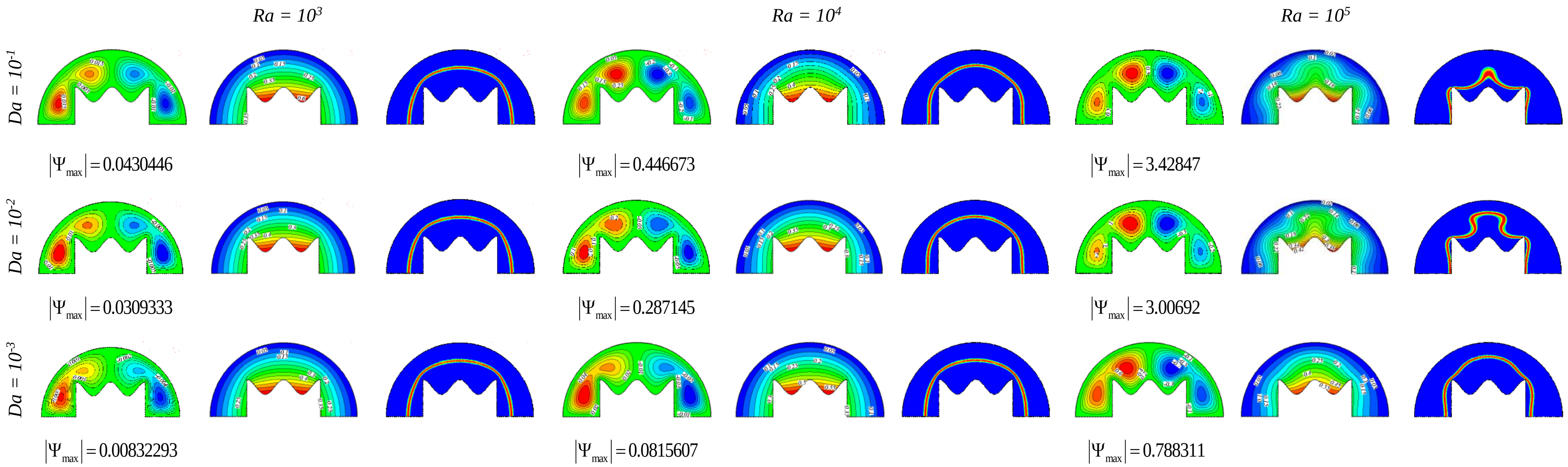

Fig. 3. θ, Ψ, and C_r for varied measure of Da and Ra when N=2, b=0.2, Hs=1 ϕ=0.05, Ste=0.313, and θ_f=0.2

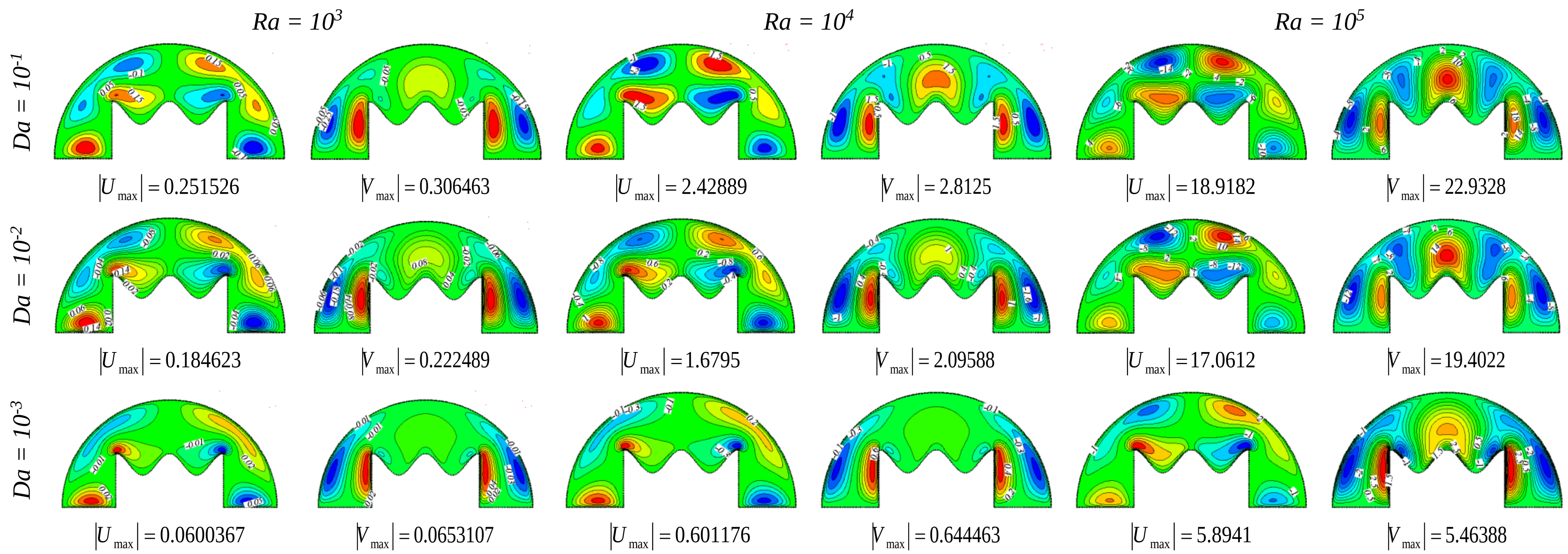

Fig. 4. U and V for varied measure of Da and Ra when N=2, b=0.2, Hs=1 ϕ=0.05, Ste=0.313, and θ_f=0.2

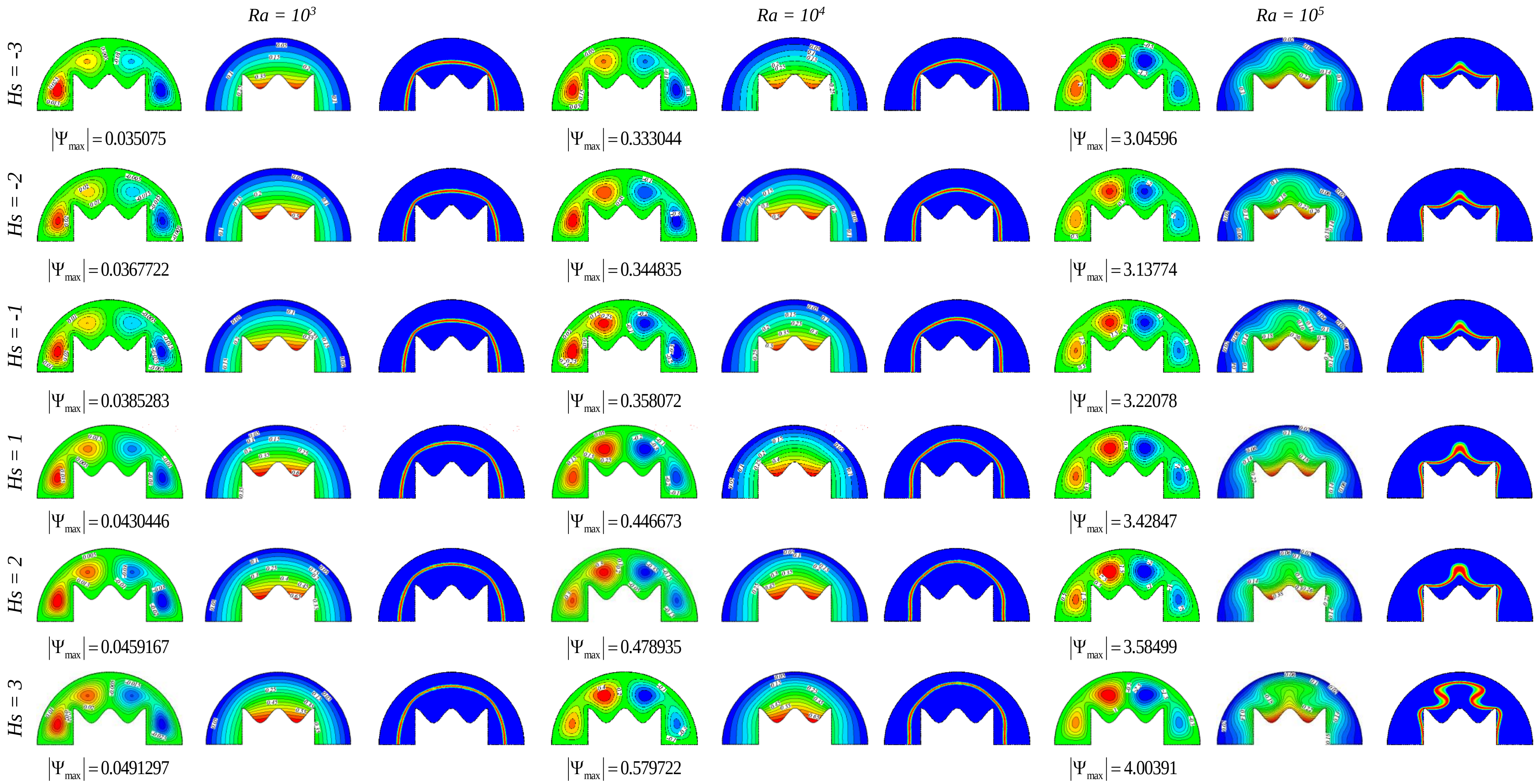

Fig. 5. θ, Ψ, and C_r for varied measure of Hs and Ra when N=2, b=0.2, Da=10^{-1} ϕ=0.05, Ste=0.313, and θ_f=0.2

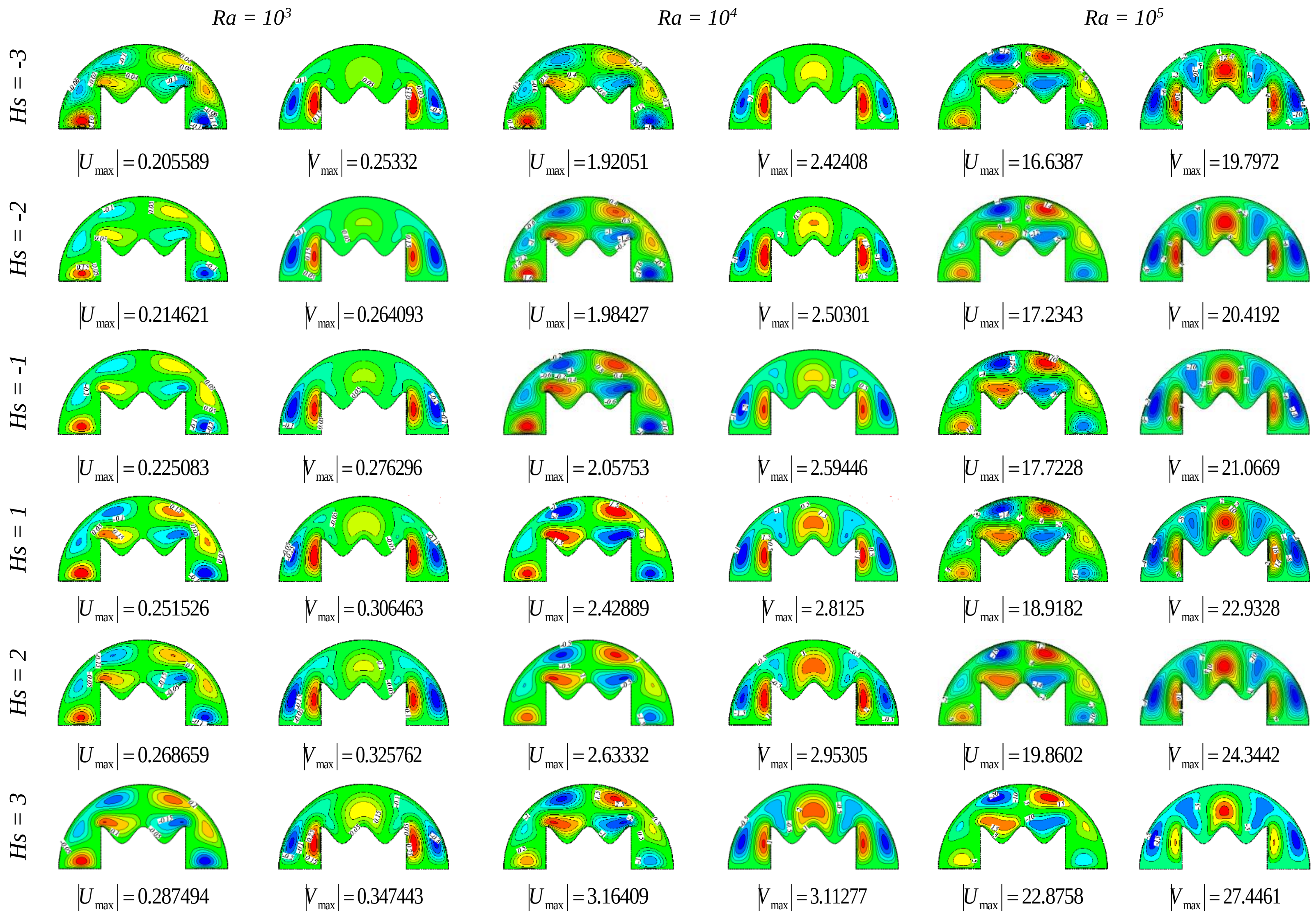

Fig. 6. U and V for varied measure of Ha and Ra when N=2, b=0.2, Da=10^{-1} ϕ=0.05, Ste=0.313, and θ_f=0.2

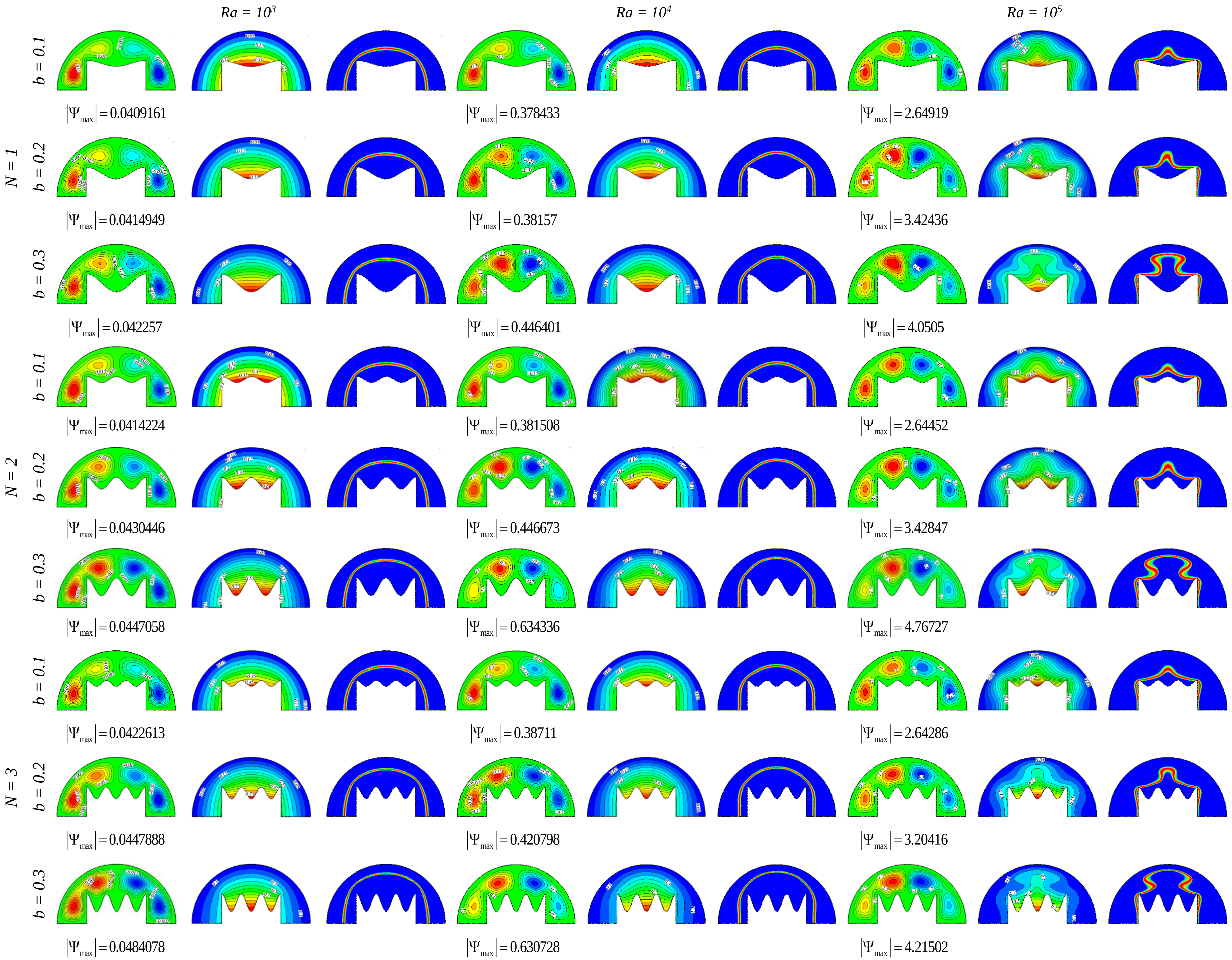

Fig. 7. θ, Ψ, and C_r for varied measure of N, b, and Ra when Hs=1, Da=10^{-1} ϕ=0.05, Ste=0.313, and θ_f=0.2

Ra = 10^3 *Ra = 10^4* *Ra = 10^5*

Fig. 8. U and V for varied measure of N, b, and Ra when Hs=1, Da=10^{-1} ϕ=0.05, Ste=0.313, and θ_f=0.2

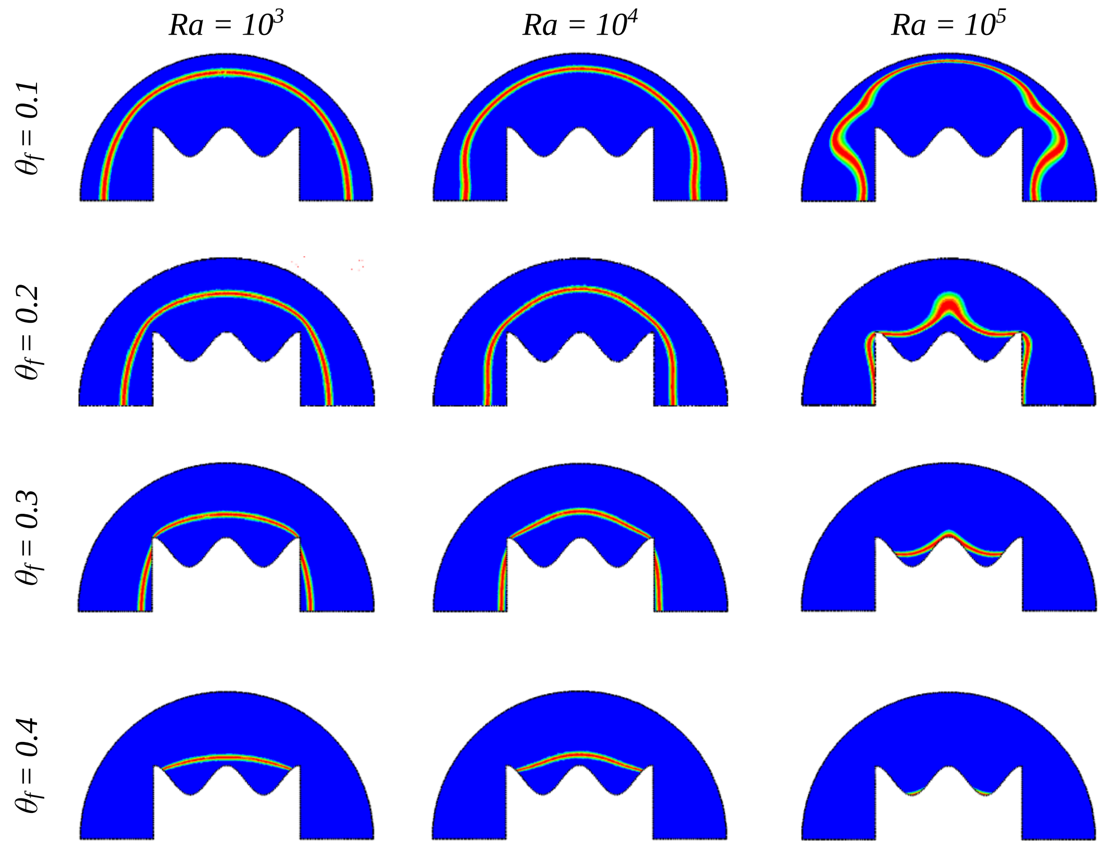

Fig. 9. C_r for varied measure of θ_f and Ra when N=2, b=0.2, Hs=1 ϕ=0.05, Ste=0.313, and Da=10^{-1}.

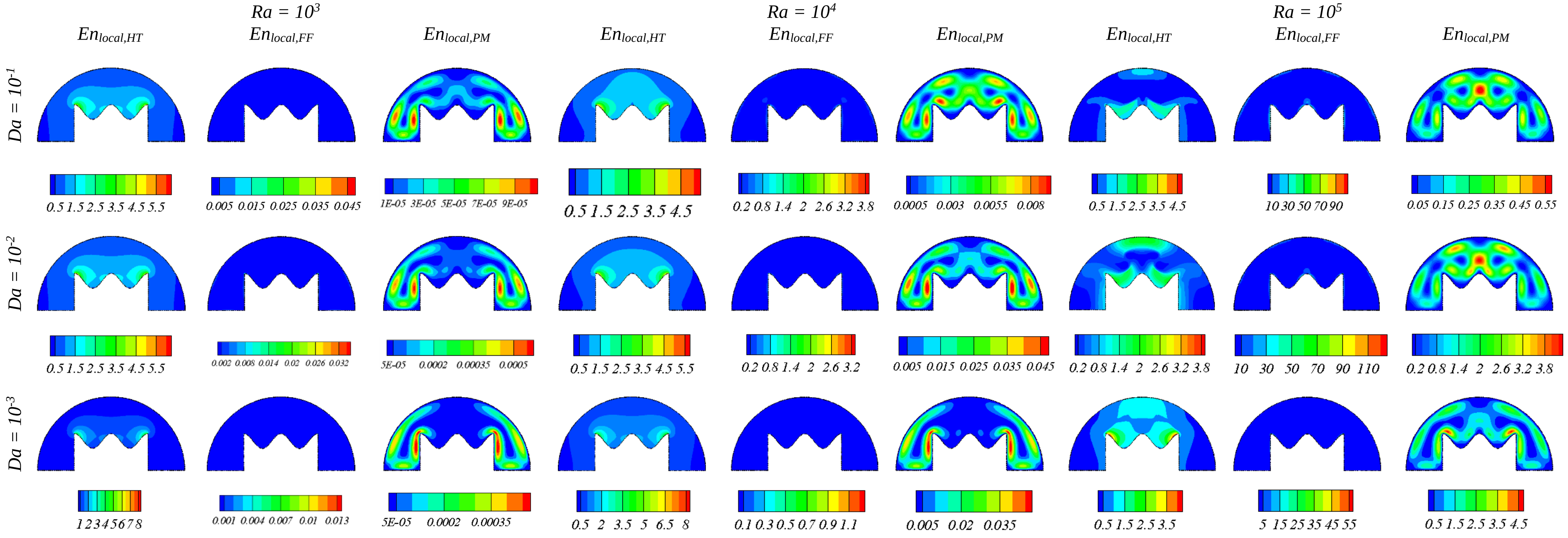

Fig. 10. $En_{local,HT}$, , $En_{local,FF}$ and $En_{local,PM}$ for varied measure of Da and Ra when N=2, b=0.2, Hs=1, ϕ=0.05, Ste=0.313, and θ_f=0.2

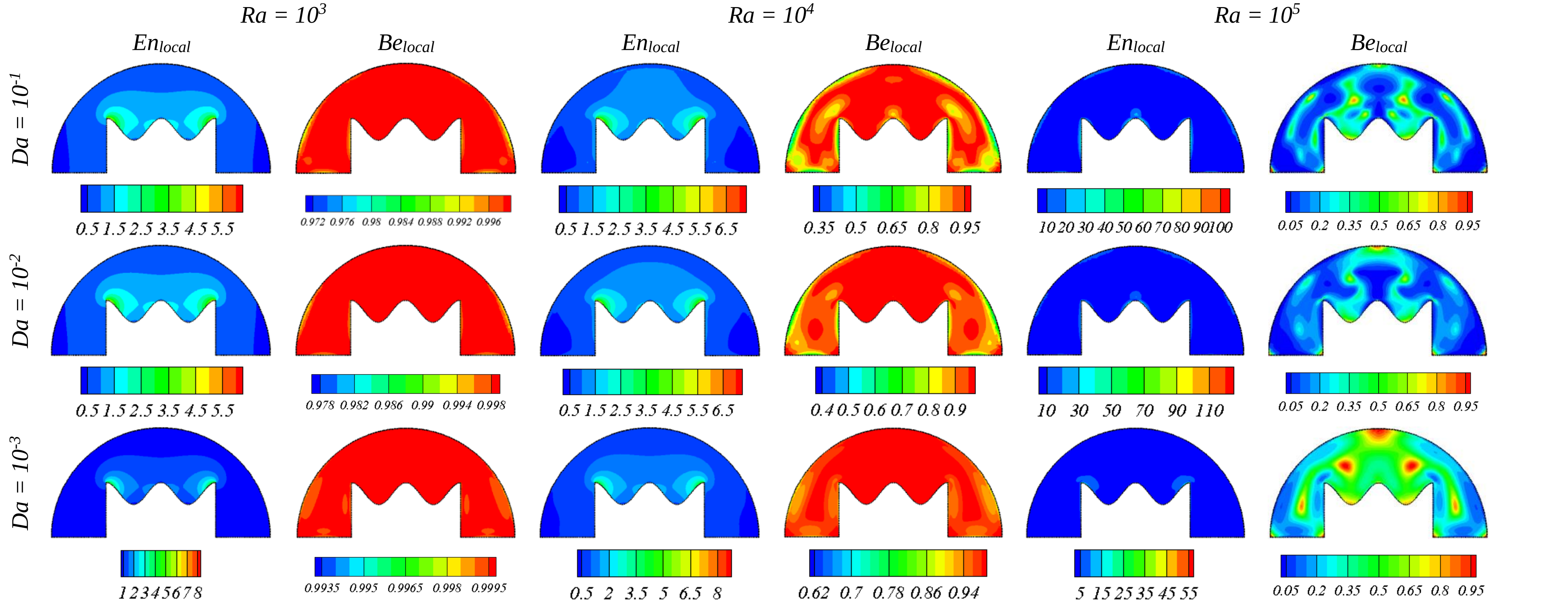

Fig. 11. En_{local} and Be_{local} for varied measure of Da and Ra when N=2, b=0.2, Hs=1, ϕ=0.05, Ste=0.313, and θ_f=0.2

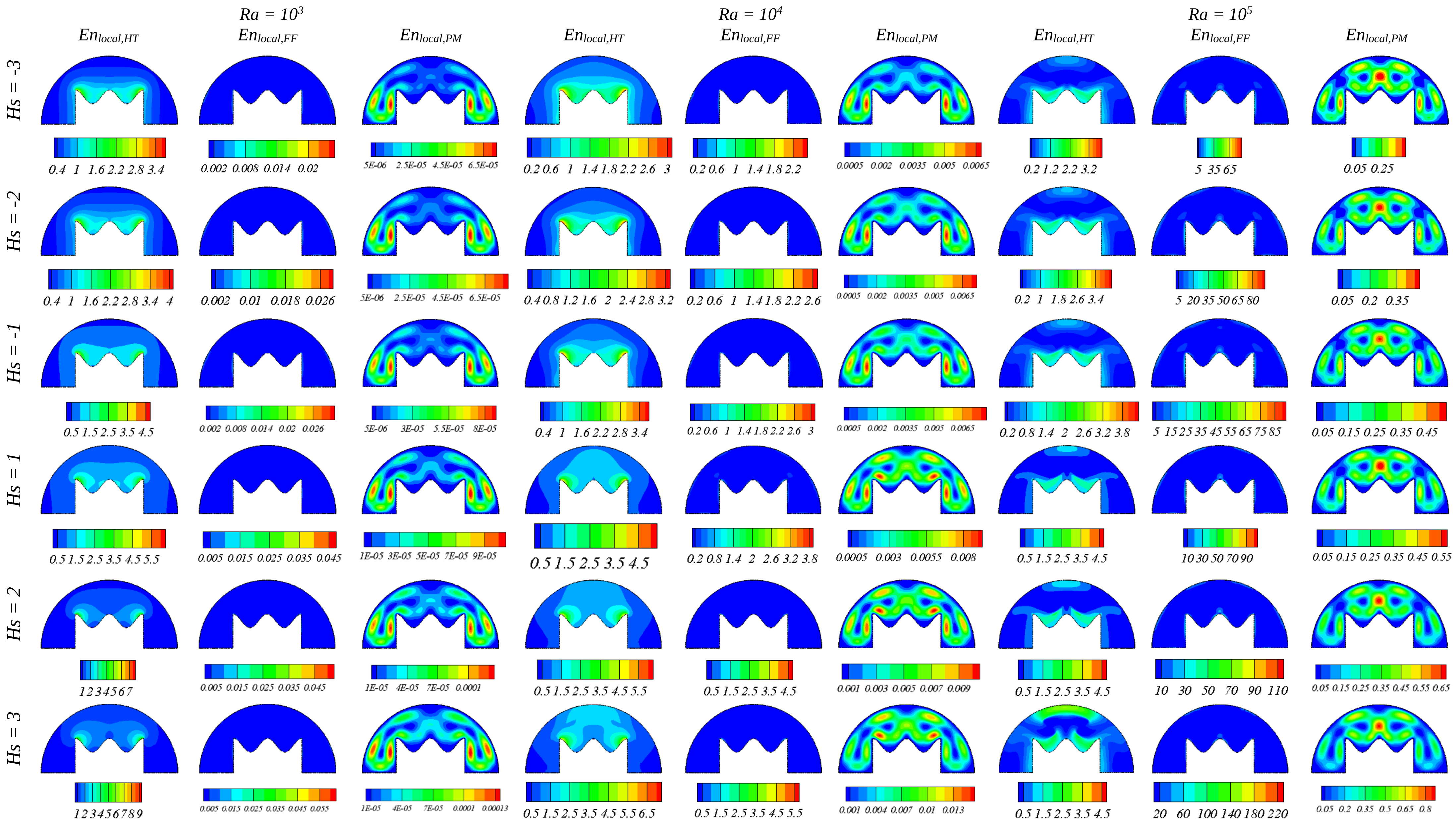

Fig. 12. $En_{local,HT}$, , $En_{local,FF}$ and $En_{local,PM}$ for varied measure of Hs and Ra when N=2, b=0.2, Da=10^{-1}, ϕ=0.05, Ste=0.313, and θ_f=0.2

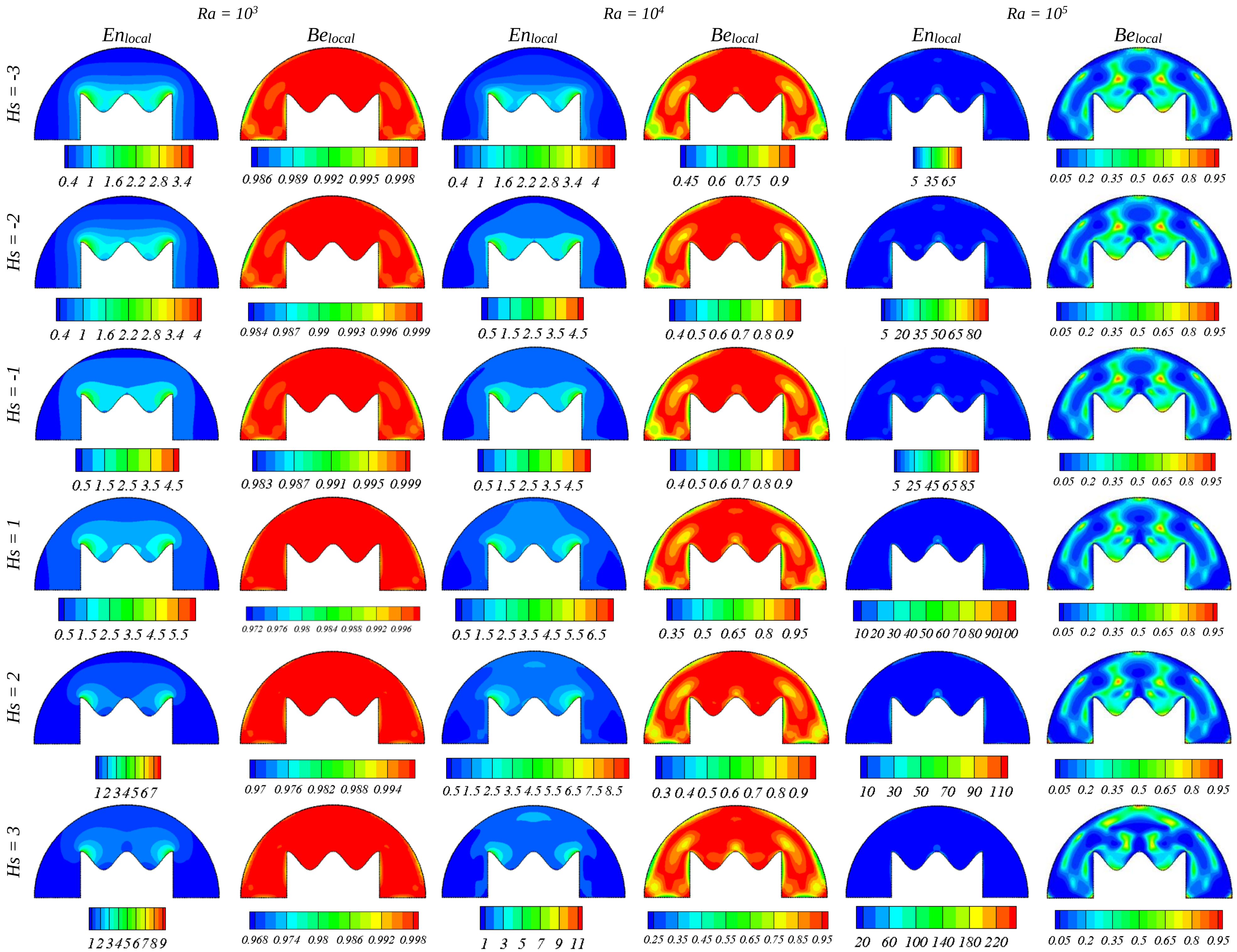

Fig. 13. En_{local} and Be_{local} for varied measure of Hs and Ra when N=2, b=0.2, Da=10^{-1}, ϕ=0.05, Ste=0.313, and θ_f=0.2

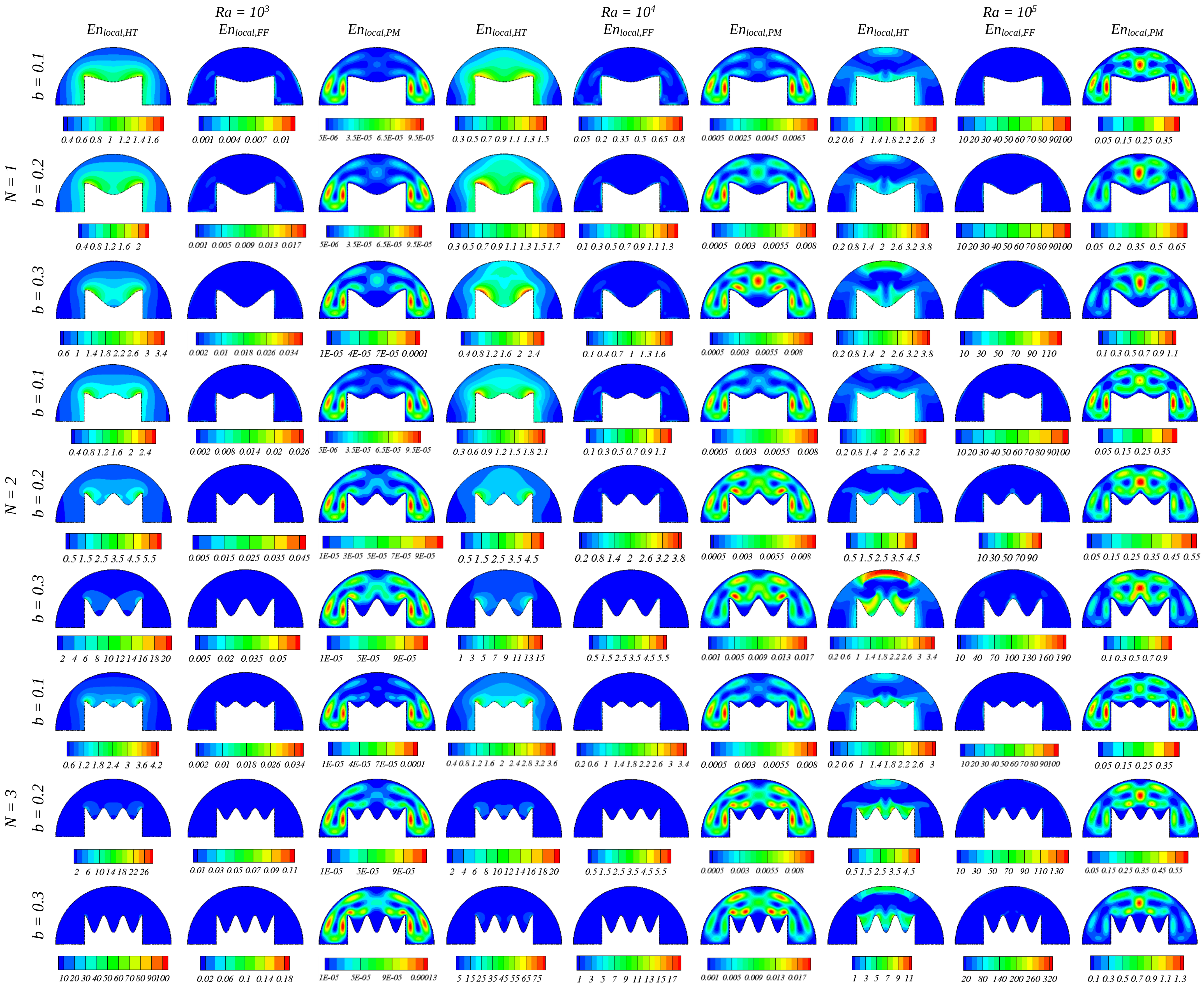

Fig. 14. $En_{local,HT}$, , $En_{local,FF}$ and $En_{local,PM}$ for varied measure of N, b, and Ra when Hs=1, Da=10^{-1} ϕ=0.05, Ste=0.313, and θ_f=0.2

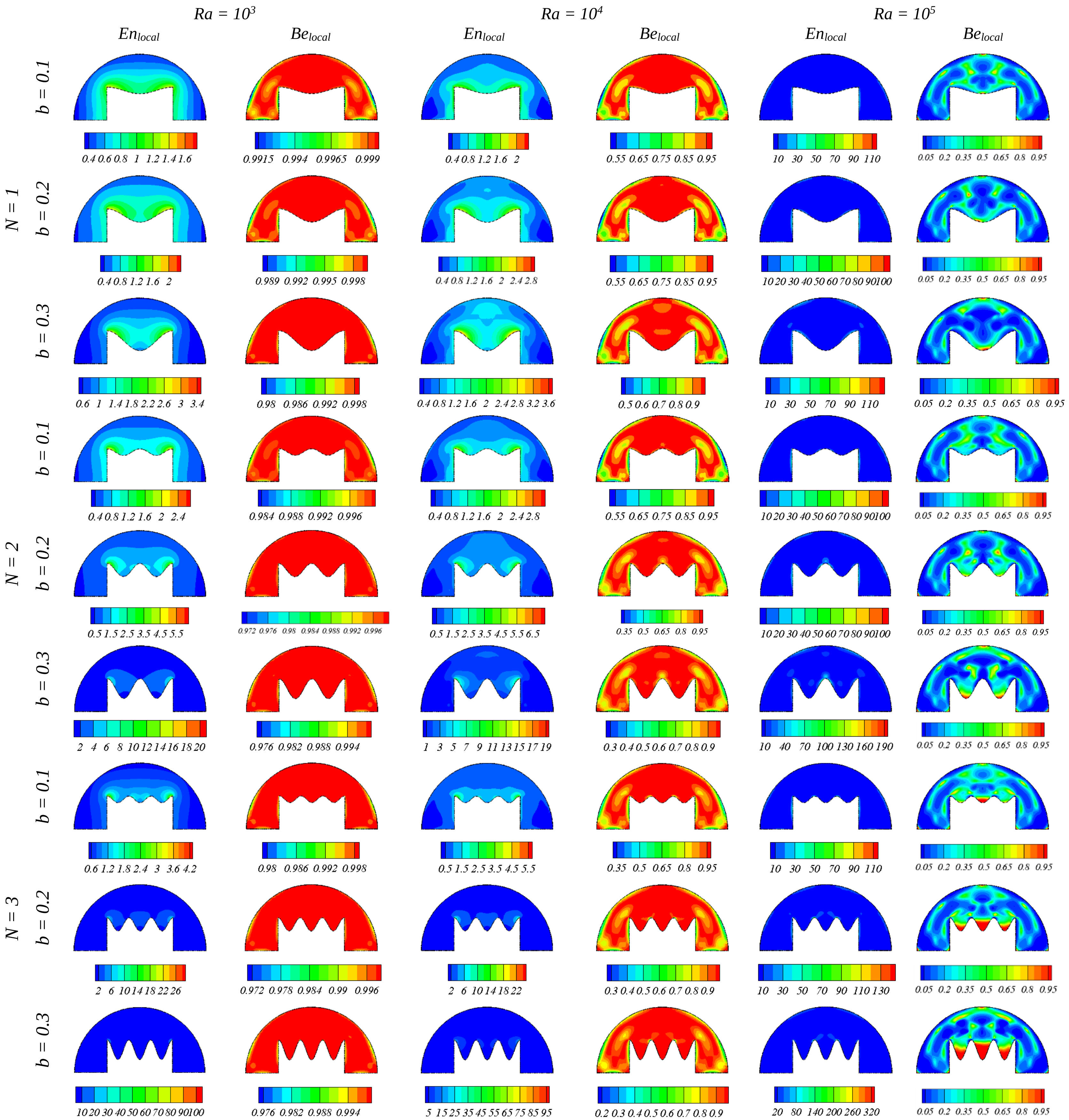

Fig. 15. En_{local} and Be_{local} for varied measure of N, b, and Ra when Hs=1, $Da=10^{-1}$ $\phi=0.05$, Ste=0.313, and $\theta_f=0.2$

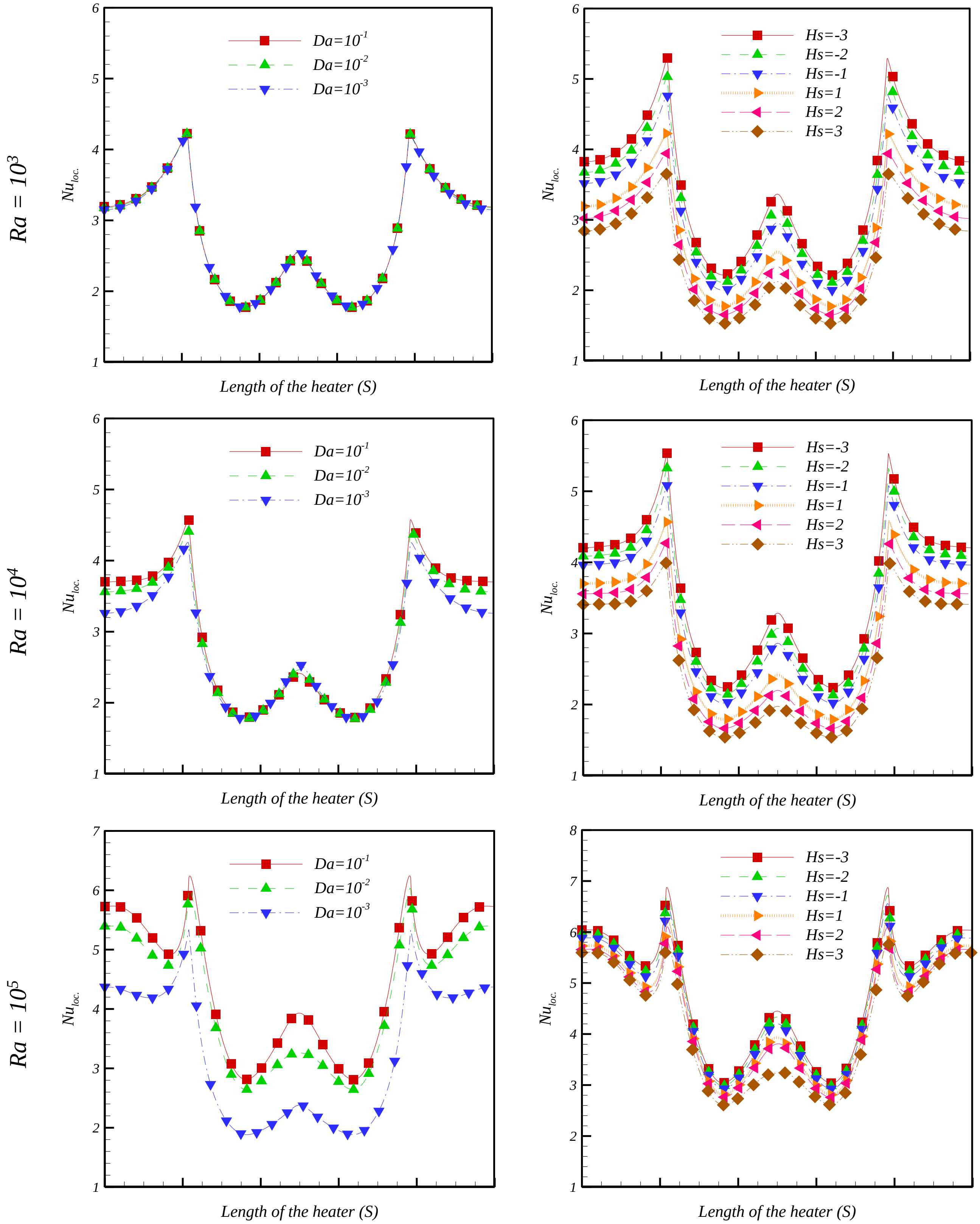

Fig. 16. Nu_{loc} for varied measure of Da, Ra, and Hs

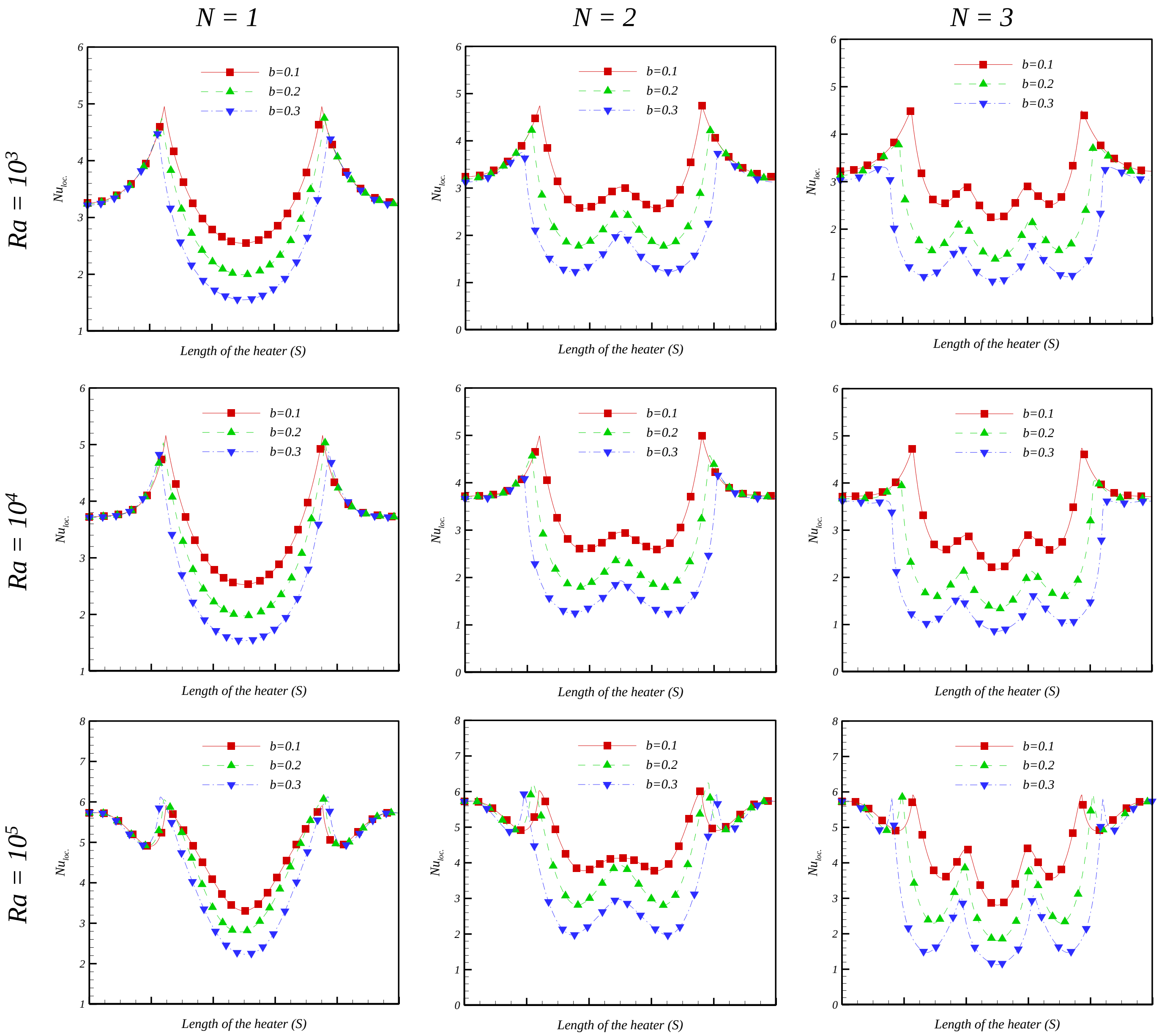

Fig. 17. Nu_{loc} for varied measure of N, b, and Ra

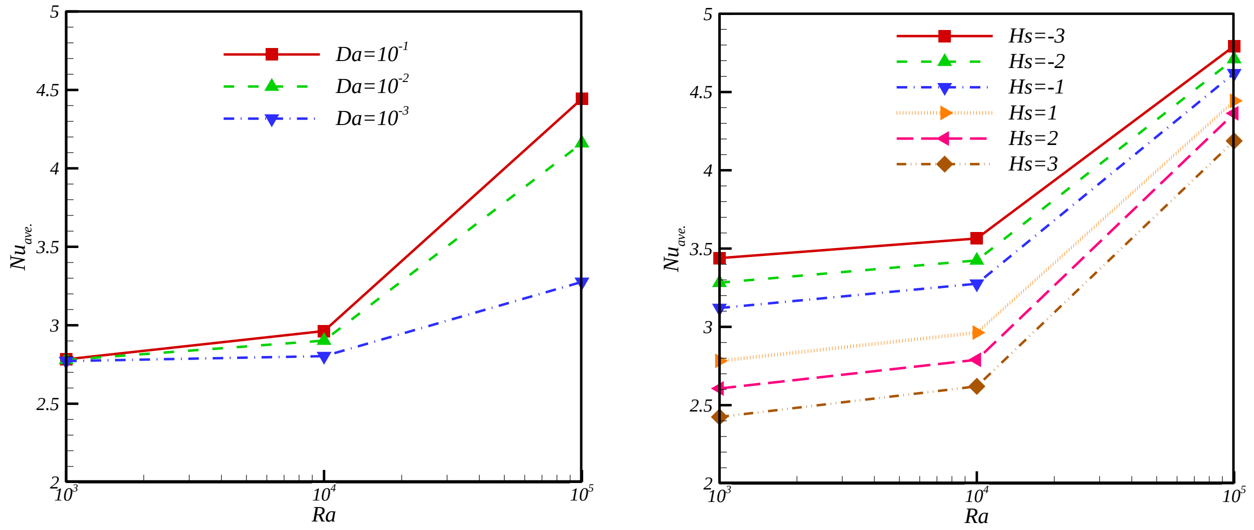

Fig. 18. $Nu_{ave.}$ for varied measure of Da, Hs and Ra

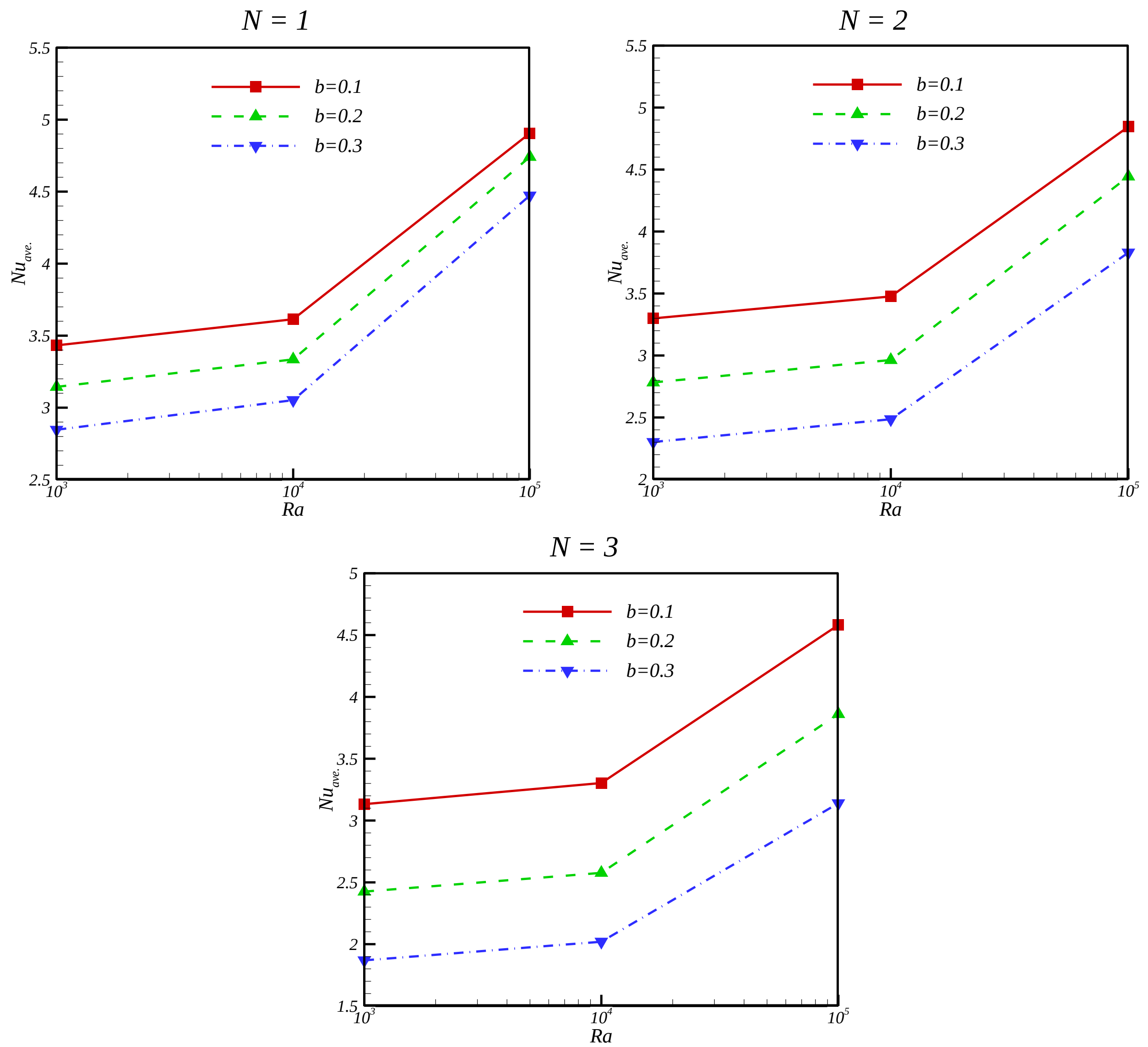

Fig. 19. $Nu_{ave.}$ for varied measure of N and b

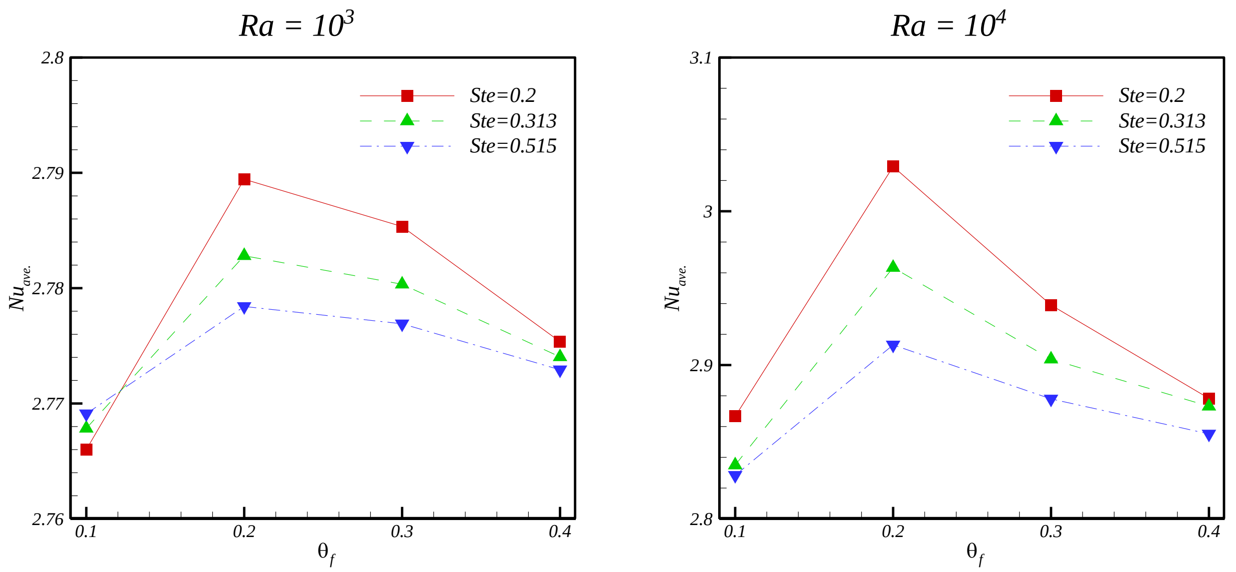

Fig. 20. $Nu_{ave.}$ for varied measure of θ_f and Ste

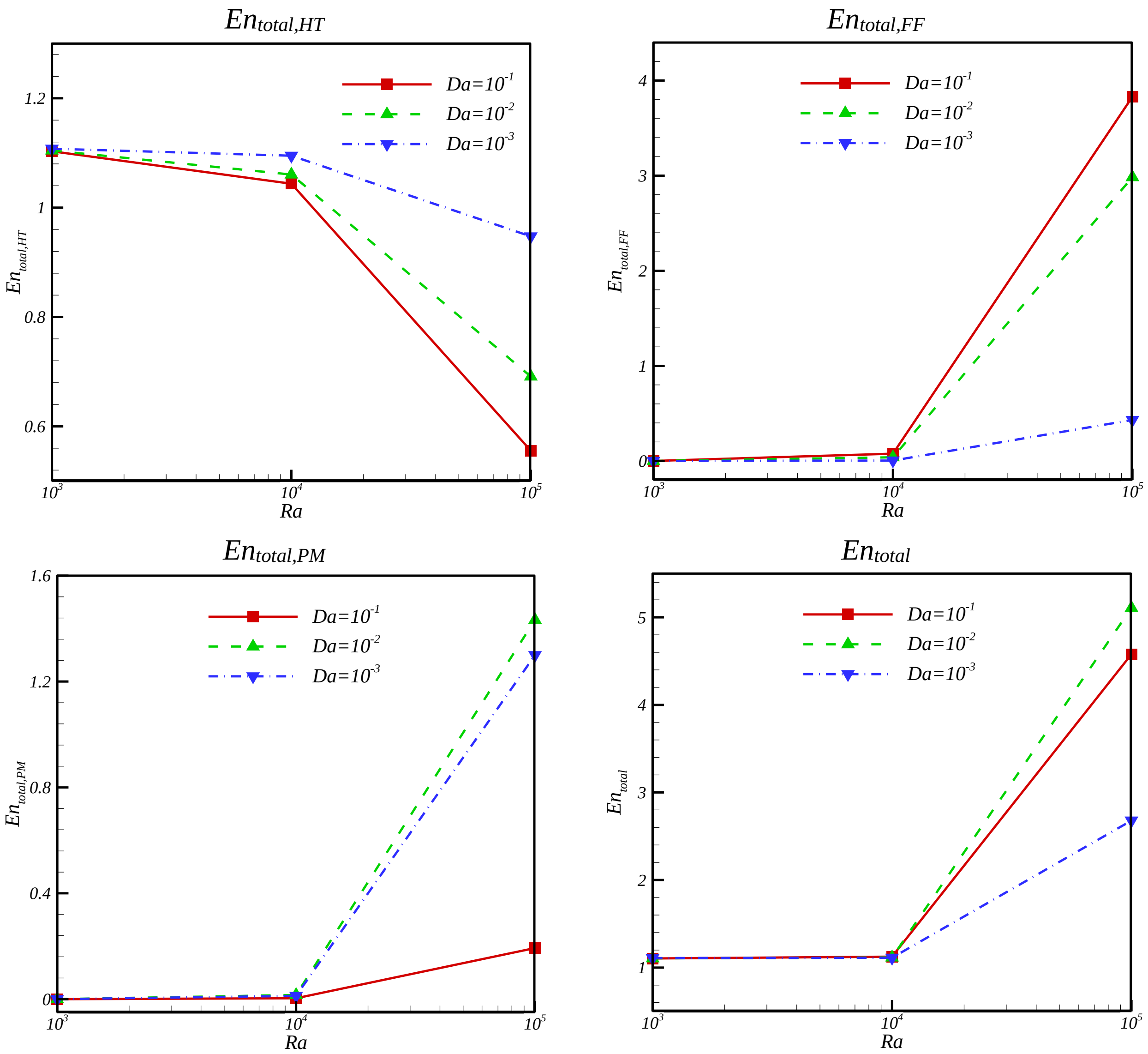

Fig. 21. $En_{total,HT}$, $En_{total,FF}$, $En_{total,PM}$, and En_{total} for varied measure of Da and Ra

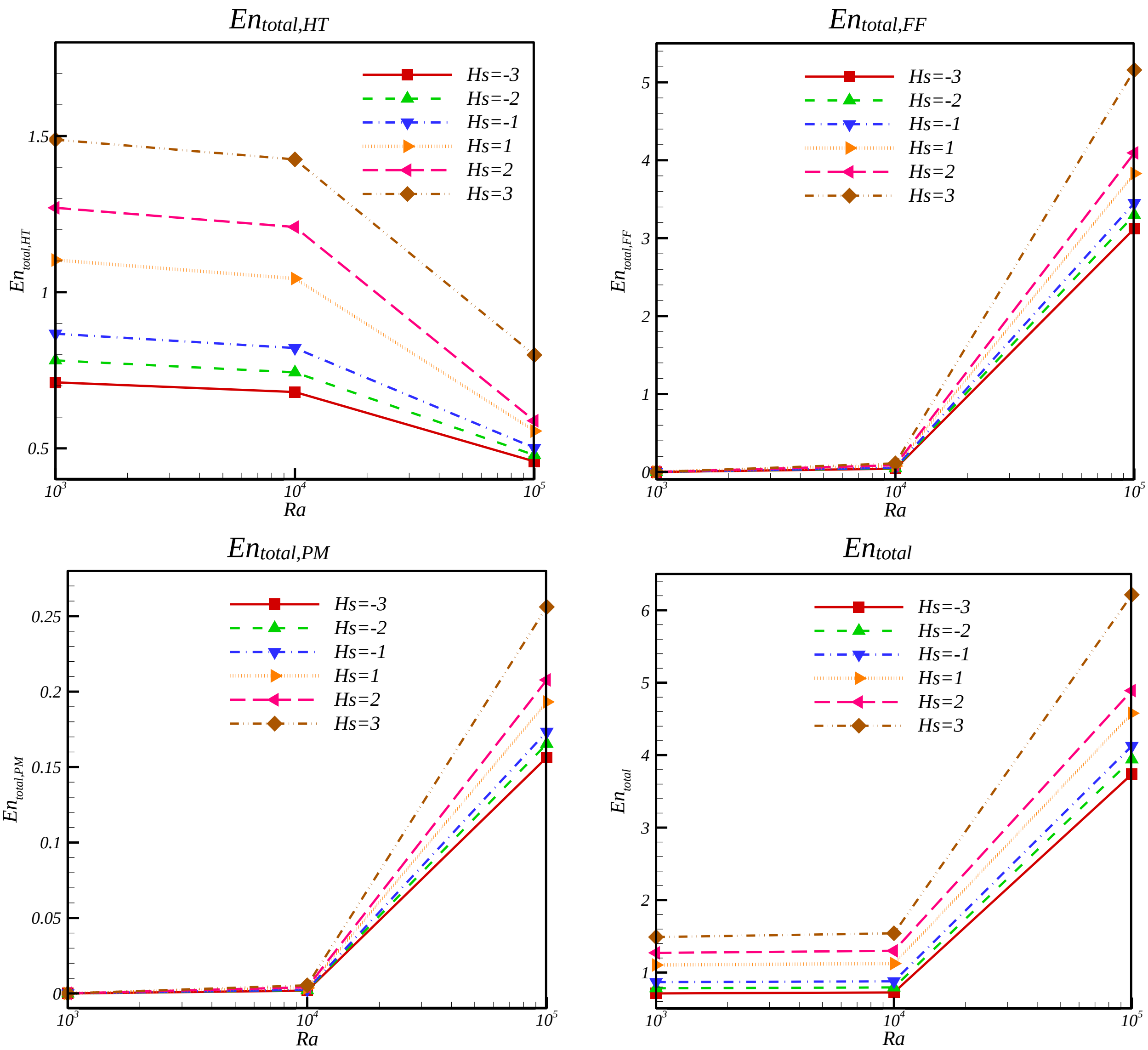

Fig. 22. $En_{total,HT}$, $En_{total,FF}$, $En_{total,PM}$, and En_{total} for varied measure of Hs

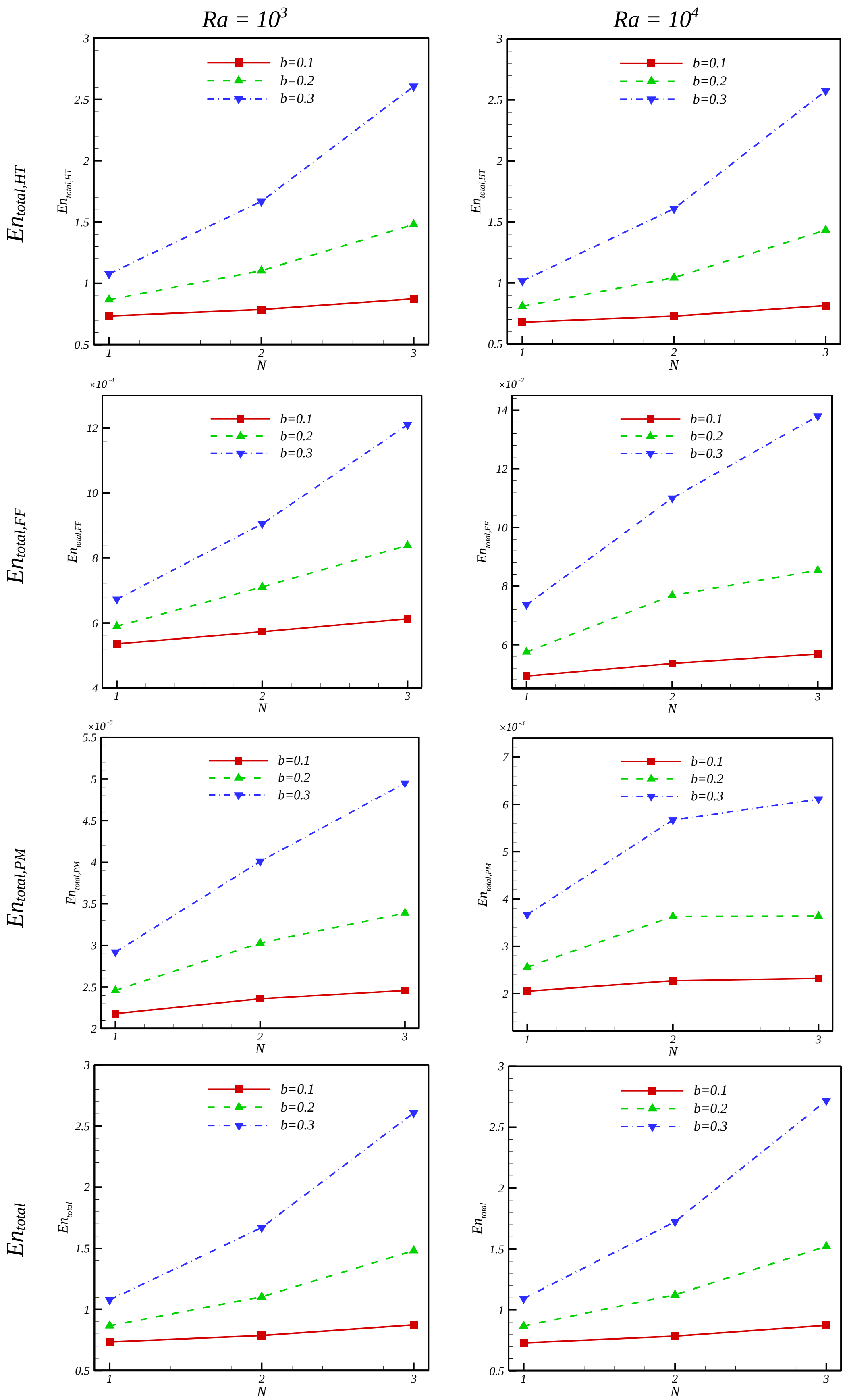

Fig. 23. $En_{total,HT}$, $En_{total,FF}$, $En_{total,PM}$, and En_{total} for varied measure of N and b

References

[1] Yousefi T, Veysi F, Shojaeizadeh E, Zinadini S. An experimental investigation on the effect of Al2O3–H2O nanofluid on the efficiency of flat-plate solar collectors. Renew Energy. 2012;39:293-8.

[2] Saidur R, Leong KY, Mohammad HA. A review on applications and challenges of nanofluids. Renew Sustain Energy Rev. 2011;15:1646–68.

[3] Leong KY, Saidur R, Kazi SN, Mamun AH. Performance investigation of an automotive car radiator operated with nanofluid- based coolants (nanofluid as a coolant in a radiator). Appl Therm Eng. 2010;30:2685–92.

[4] Seyyedi SM, Dogonchi AS, Ganji DD, Hashemi-Tilehnoee M. Entropy generation in a nanofluid-filled semi-annulus cavity by considering the shape of nanoparticles. Journal of Thermal Analysis and Calorimetry 2019;138:1607-21.

[5] Ghasemi B, Aminossadati SM. Brownian motion of nanoparticles in a triangular enclosure with natural convection. Int J Therm Sci. 2010;49:931–40.

[6] Ghasemi B, Aminossadati SM. Natural convection heat transfer in an inclined enclosure filled with a water–CuO nanofluid. Numer Heat Transf Part A Appl. 2009;55:807–23.

[7] Sheremet MA, Cimpean DS, Pop I. Free convection in a partially heated wavy porous cavity filled with a nanofluid under the effects of Brownian diffusion and thermophoresis. App. Therm. Eng. 2017;113:413-18.

[8] Izadi M, Mohebbi R, Chamkha AJ, Pop I, Effects of cavity and heat source aspect ratios on natural convection of a nanofluid in a C-shaped cavity using Lattice Boltzmann method, Int. J. Numer. Methods Heat Fluid Flow 2018;28:1930-55.

[9] Ahmed SE, Aly AM. Natural convection in a nanofluid-filled cavity with solid particles in an inner cross shape using ISPH method. Int. J. Heat Mass Transf. 2019;141:390-406.

[10] Ma Y, Mohebbi R, Rashidi MM, Yang Z. Effect of hot obstacle position on natural

convection heat transfer of MWCNTs-water nanofluid in U-shaped enclosure using lattice Boltzmann method. Int. J. Numer. Methods Heat Fluid Flow 2019;29:223-50.

[11] Sivaraj C, Sheremet MA. MHD natural convection and entropy generation of ferrofluids in a cavity with a non-uniformly heated horizontal plate. Int. J. Mech. Sci. 2018;149:326-37.

[12] Seyyedi SM. On the entropy generation for a porous enclosure subject to a magnetic field: Different orientations of cardioid geometry. Int. Commun. Heat Mass Transfer 2020;116:104712.

[13] Gholamalipour P, Siavashi M, Doranehgard MH. Eccentricity effects of heat source inside a porous annulus on the natural convection heat transfer and entropy generation of Cu-water nanofluid. Int. Commun. Heat Mass Transfer 2019;109:104367.

[14] Selimefendigil F, Oztop HF. Natural convection and entropy generation of nanofluid filled cavity having different shaped obstacles under the influence of magnetic field and internal heat generation. J. Taiwan Inst. Chem. Eng. 2015;56:42-56.

[15] Rashad AM, Armaghani T, Chamkha AJ, Mansour MA. Entropy generation and MHD natural convection of a nanofluid in an inclined square porous cavity: Effects of a heat sink and source size and location. Chinese Journal of Physics 2018;56:193-211.

[16] Cho CC, Chen CL, Chen CK. Natural convection heat transfer performance in complex-wavy-wall enclosed cavity filled with nanofluid. Int J Therm Sci. 2012;60:255–63.

[17] Tayebi T, Oztop HF. Entropy production during natural convection of hybrid nanofluid in an annular passage between horizontal confocal elliptic cylinders. Int. J. Mech. Sci. 2020;171:105378.

[18] Su, Darkwa WJ, Kokogiannakis G, Review of solid–liquid phase change materials and their encapsulation technologies, Renew. Sustain. Energy Rev. 2015;48:373-91.

[19] Ghalambaz M, Chamkha AJ, Wen D. Natural convective flow and heat transfer of Nano-Encapsulated Phase Change Materials (NEPCMs) in a cavity. Int. J. Heat Mass Transf. 2019;138:738-49.

[20] Raizah Z, Aly AM. Double-diffusive convection of a rotating circular cylinder in a porous cavity suspended by nano-encapsulated phase change materials. Case Stud. Therm. Eng. 2021;24:100864.

[21] Seyf HR, Zhou Z, Ma HB, Zhang Y. Three dimensional numerical study of heat-transfer enhancement by nano-encapsulated phase change material slurry in microtube heat sinks with tangential impingement. Int. J. Heat Mass Tran. 2013;56:561-73.

[22] Ghalambaz M, Mehryan SAM, Mozaffari M, Hajjar A, Kadri ME, Rachedi N, Sheremet M, Younis O, Nadeem S. Entropy generation and natural convection flow of a suspension containing nano-encapsulated phase change particles in a semi-annular cavity. J. Energy Storage 2020;32:101834.

[23] Mehryan SAM, Ghalambaz M, Gargari LS, Hajjar A, Sheremet M. Natural convection flow of a suspension containing nano-encapsulated phase change particles in an eccentric annulus. J. Energy Storage 2020;28:101236.

[24] Dogonchi AS, Mishra SR, Karimi N, Chamkha AJ, Alhumade H. Interaction of fusion temperature on the magnetic free convection of nano-encapsulated phase change materials within two rectangular fins-equipped porous enclosure. J. Taiwan Inst. Chem. Eng. 2021. https://doi.org/10.1016/j.jtice.2021.03.010

[25] Seyyedi SM, Dogonchi AS, Hashemi-Tilehnoee M, Ganji DD, Chamkha AJ. Second law analysis of magneto-natural convection in a nanofluid filled wavy-hexagonal porous enclosure. Int. J. Numer. Methods Heat Fluid Flow 2020;30:4811-36.

[26] Usman M, Khan ZH, Liu MB. MHD natural convection and thermal control inside a cavity with obstacles under the radiation effects. Physica A 2019;535:122443.

[27] Krane RJ, Jessee J. Some detailed field measurements for a natural convection flow in a vertical square enclosure. In: Proceedings of the first ASME-JSME thermal engineering joint conference, 1; 1983. p. 323–9.

[28] Khanafer K, Vafai K, Lightstone M. Buoyancy-driven heat transfer enhancement in a two-dimensional enclosure utilizing nanofluids. Int J Heat Mass Transf 2003;46:3639–53.

Graphical Abstract:

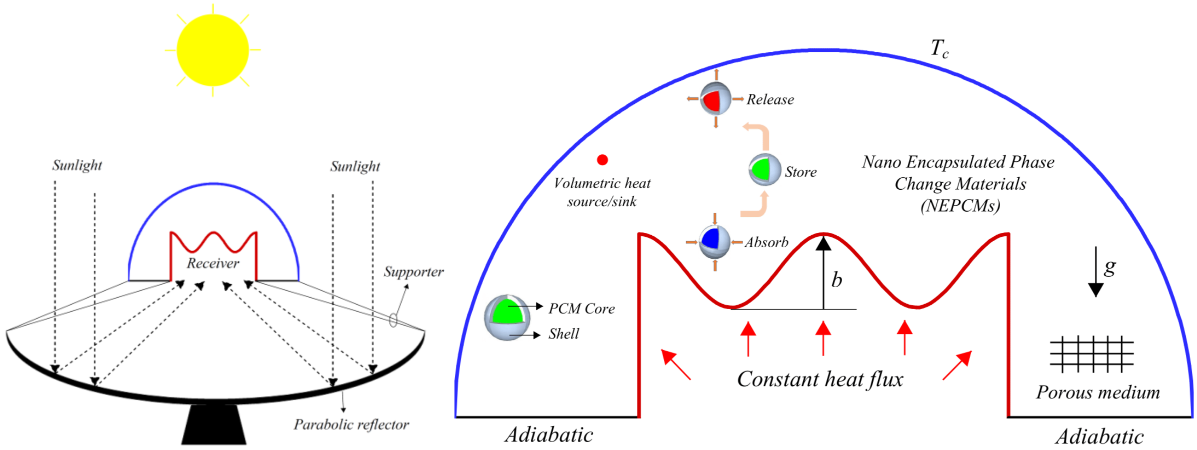

Declaration of interests

☒ The authors declare that they have no known competing financial interests or personal relationships that could have appeared to influence the work reported in this paper.

☐The authors declare the following financial interests/personal relationships which may be considered as potential competing interests: